

¹ Characterizing the Splice Map of Turkey Hemorrhagic Enteritis
² Virus

³

⁴ Abraham Quaye^{†,a}, Brett E. Pickett^a, Joel S. Griffitts^a, Bradford K. Berges^a, Brian D. Poole^{a,*}

⁵ ^aDepartment of Microbiology and Molecular Biology, Brigham Young University

⁶ [†]First-author

⁷ ^{*}Corresponding Author

⁸ **Corresponding Author Information**

⁹ brian_poole@byu.edu

¹⁰ Department of Microbiology and Molecular Biology,

¹¹ 4007 Life Sciences Building (LSB),

¹² Brigham Young University,

¹³ Provo, Utah

¹⁴

15 **ABSTRACT**

16 Characterizing the splice map of turkey hemorrhagic enteritis virus (THEV) is an essential step that would
17 allow studies of individual genes mediating its immunosuppressive functions. We used RNA sequencing
18 to characterize the transcriptome of THEV for the first time, providing key insights into the THEV gene
19 expression and mRNA structures. Researchers previously annotated the genome of THEV as encoding
20 23 open reading frames (ORFs). In this work we identified 29 spliced transcripts all of which contained
21 novel exons although some exons matched some previously annotated ORFs. The three annotated splice
22 junctions were also corroborated by our data. We performed PCR amplification of THEV cDNA, cloned the
23 PCR products, and used Sanger sequencing to validate all identified splice junctions. During validation we
24 identified five additional unique transcripts, a subset of which were further validated by 3' rapid amplification
25 of cDNA ends (3' RACE) experiments. Thus, we report that the genome of THEV contains 34 transcripts
26 with the coding capacity for all annotated ORFs. However, we found six of the previously annotated ORFs
27 (ORF1, E3, 33K, ORF8, IVa2, and protease) to be truncated ORFs on the basis of the identification of an
28 in-frame upstream start codon or the detection of additional coding exons. We also identified three of the
29 annotated ORFs with longer or shorter isoforms, and seven novel unannotated ORFs that could potentially
30 be translated; although it is beyond the scope of this manuscript to investigate whether they are translated.
31 Similar to other adenoviruses (AdVs), THEV also produces multiple distinctly spliced transcripts that code for
32 the same protein. Our data show that all THEV transcripts are spliced and organized into five transcription
33 units under the control of their cognate promoters like other AdVs.

34 INTRODUCTION

35 Adenoviruses (AdVs) are non-enveloped icosahedral-shaped DNA viruses, causing infection in virtually all
36 types of vertebrates studied to date. Their double-stranded linear DNA genomes range between 26 and
37 45kb in size, producing a broad repertoire of transcripts via highly complex alternative splicing patterns (1,
38 2). The AdV genome is one of the most optimally economized; both the forward and reverse DNA strands
39 harbor protein-coding genes, making it highly gene-dense. There are 16 genes termed “genus-common”
40 that are homologous in all AdVs, presumably inherited from a common ancestor. All other genes are termed
41 “genus-specific”. The genus-specific genes tend to be located at the termini of the genome while genus-
42 common genes are usually towards the center of the genome (1). This pattern is also observed in *Poxviridae*
43 and *Herpesviridae*, which also have linear DNA genomes (1, 3, 4). The family *Adenoviridae* consists of five
44 genera: *Mastadenovirus* (MAdV), *Aviadenovirus*, *Atadenovirus*, *Ichtadenovirus*, and *Siadenovirus* (SiAdV) to
45 which turkey adenovirus 3 also called turkey hemorrhagic enteritis virus (THEV) belongs (5–10). Members of
46 SiAdV have the smallest genome size (~26 kb) and gene content of all known AdVs (see **Figure 1**) (1, 2, 6).

47 Virulent THEV strains (THEV-V) and avirulent strains (THEV-A) of THEV both infect turkeys, with THEV-
48 V causing hemorrhagic enteritis (HE), a debilitating acute disease predominantly affecting turkey pouls
49 characterized by immunosuppression, intestinal lesions leading to bloody diarrhea, and up to 80% mortality
50 (2, 11–13). While the current vaccine strain (a THEV-A called Virginia Avirulent Strain [VAS]) has proven
51 effective at preventing HE in turkey pouls, it still retains its immunosuppressive ability. Thus, vaccinated
52 birds are rendered more susceptible to opportunistic infections and death than unvaccinated birds leading to
53 substantial economic losses (11, 14–16). To eliminate the immunosuppressive effect of the vaccine strain,
54 a thorough investigation of the culprit viral genes mediating this phenomenon is essential. However, the
55 transcriptome (splicing and gene expression patterns) of THEV has not been characterized, making an
56 investigation of specific immunosuppressive viral genes impractical.

57 A myriad of studies have elucidated the AdV transcriptome in fine detail (17, 18). However, a large
58 preponderance of studies focus on MAdVs – specifically human AdVs. Thus, most of the current AdV gene
59 expression and replication knowledge is based on MAdV studies, which is generalized for all other AdVs (10,
60 19). MAdV transcription is temporally regulated; their genes are categorized into five early transcription units
61 (E1A, E1B, E2, E3, and E4), two intermediate (IM) units (pIX and IVa2), and one major late transcription unit
62 (MLTU or major late promoter [MLP] region), which generates five families of late mRNAs (L1-L5) based on
63 the polyadenylation site. An additional gene (UXP or U exon) is located on the reverse strand. The early
64 genes encode non-structural proteins such as enzymes or host-cell modulating proteins, primarily involved
65 in DNA replication, or providing the necessary intracellular niche for optimal replication while late genes

66 encode structural proteins that act as capsid proteins, promote virion assembly, or direct genome packaging.
67 The immediate early genes E1A are expressed first, followed by the delayed early genes, E1B, E2, E3 and
68 E4. Then the intermediate early genes, IVa2 and pIX are expressed followed by the late genes (10, 17,
69 18). It is noteworthy that the MLP shows basal transcriptional activity during early infection (before DNA
70 replication), with a comparable efficiency to other early viral promoters, but it reaches its maximal activity
71 during late infection (after DNA replication). However, during early infection only a subset of the MLP-derived
72 transcripts are expressed (10). MAdV makes an extensive use of alternative RNA splicing to produce a very
73 complex array of mRNAs. All but the pIX mRNA undergo at least one splicing event. For instance, the MLTU
74 produces over 20 distinct splice variants all containing three non-coding exons at the 5'-end (collectively
75 known as the tripartite leader; TPL) (17, 18). There is also an alternate three-exon 5' non-coding leader
76 sequence present in varying amounts on a subset of MLTU mRNAs (known as the x-, y-, and z-leaders).
77 Lastly, there is the i-leader exon, which is infrequently included between the second and third TPL exons,
78 and codes for the i-leader protein (20). Thus, the MLTU produces a complex repertoire of mRNA with diverse
79 5' untranslated regions (UTRs) spliced onto different 3' coding exons which are grouped into five different
80 3'-end classes (L1-L5) based on polyadenylation site. Each transcription unit (TU) contains its own promoter
81 driving the expression of the array of mRNA transcripts produced via alternative splicing in the unit (10, 17,
82 18). The promoters are activated at different phases of infection by proteins from previously activated TUs.
83 Paradoxically, the early-to-late phase transition during infection requires the L4 gene products, 22K and 33K,
84 which should only be available after the transition. However, a promoter in the L4 region (L4P) that directs
85 the expression of these two proteins independent of the MLP was found, resolving the paradox (10, 17, 21).
86 During translation of AdV mRNA, recent studies using long-read direct RNA sequencing strongly suggest
87 the potential usage of secondary start codons; adding to what was already a highly complex system for gene
88 expression (17, 22).
89 High throughput sequencing methods have facilitated the discovery of many novel transcribed regions and
90 splicing isoforms. It is also a very powerful tool to study alternative splicing under different conditions at
91 an unparalleled depth (18, 22, 23). In this paper, we use a paired-end deep sequencing experiment to
92 characterize, for the first time, the transcriptome and splicing of THEV (VAS vaccine strain) during different
93 phases of the infection. Our paired-end sequencing allowed for reading 149 bp long high quality (mean
94 Phred Score of 36) sequences from each end of cDNA fragments, which were mapped to the genome of
95 THEV.

96 **RESULTS**

97 **Overview of sequencing data and analysis pipeline outputs**

98 A prior study by Aboeazz *et al.* demonstrated that nearly all THEV transcripts became detectable starting
99 at 4 hours post-infection (hpi), with one replication cycle concluding around 18 hpi (24). Consequently,
100 we harvested infected MDTC-RP19 cells (MOI of 100 genome copy numbers/cell) at 4-, 12-, 24-, and
101 72-hpi to capture all transcripts within a broad time window. Our paired-end RNA sequencing (RNA-seq)
102 experiment generated an average of 107.1 million total reads of 149 bp length per time-point. These reads
103 were concurrently mapped to both the virus (THEV) and host (*Meleagris gallopavo*) genomes using the
104 Hisat2 (25) reference-based aligner. A total of 18.1 million reads from all time-points mapped to the virus
105 genome, providing comprehensive coverage and leaving no regions unmapped. The mapped reads to the
106 virus genome increased significantly from a scant 432 reads at 4 hpi to 16.9 million reads at 72 hpi (**Table**
107 **1, Figure 2A**). From these mapped reads, we identified 2,457 unique THEV splice junctions across all
108 time-points, with later time-points exhibiting significantly more sequence reads supporting the splice junctions
109 than earlier time-points. For instance, all 13 unique junctions at 4 hpi had fewer than 10 supporting reads
110 each, averaging only 2.8 reads per junction. In contrast, the 2374 unique junctions at 72 hpi averaged 898.4
111 reads per junction, with some junctions reaching as high as 322,677 reads. The marked increase in splice
112 junction and mapping reads to the THEV genome over time indicates an active infection and successful viral
113 replication, which is corroborated by our quantitative PCR (qPCR) assay that quantified the total number of
114 viral genome copies over time (**Figure 2B**).

115 Using StringTie (25), we assembled the data into potential transcripts, guided by the genomic locations of
116 the previously predicted THEV ORFs. In the consolidated transcriptome, a composite of all non-redundant
117 transcripts across all time points, we identified a total of 29 novel transcripts. We found that a subset of
118 exons in the viral transcripts match some predicted ORFs exactly, with the majority of the exons being longer
119 and spanning multiple predicted ORFs (**Figure 3**).

120 We then validated the splice junctions in all transcripts by PCR amplification of viral cDNA, cloning, and Sanger
121 sequencing (**Supplementary PCR methods**). During validation, we identified five additional transcripts,
122 some of which were further validated by 3' Rapid Amplification of cDNA Ends (3' RACE) data. The complete
123 list of unique splice junctions mapped to the THEV genome has been submitted to the National Center for
124 Biotechnology Information Gene Expression Omnibus (<http://www.ncbi.nlm.nih.gov/geo>) under accession
125 number GSE254416.

126 **Changes in THEV splicing profile over time**

127 AdV gene expression is subject to meticulous temporal regulation, with each promoter typically generating
128 one or a few pre-mRNAs. These pre-mRNAs undergo alternative splicing to produce a diverse array of
129 mature mRNAs. To assess the temporal activity of each promoter, we utilized StringTie and Ballgown (a tool
130 for statistical analysis of assembled transcriptomes) (26). These tools estimated the normalized expression
131 levels of all transcripts at each time point, measured in Fragments Per Kilobase of transcript per Million
132 mapped reads (FPKM) units. At 4 hpi, we counted very few unique splice junctions, reads, and transcripts;
133 hence, this time-point was excluded from this analysis.

134 Examining individual mRNAs, TRXPT_21 – from the E2 region – was the most significantly expressed at
135 12 hpi, constituting 33.58% of the total expression of all transcripts. Transcripts in the E3 and E4 regions
136 also contributed substantial proportions, along with some MLP region transcripts. The later time points were
137 dominated by the MLP region transcripts — TRXPT_10 and TRXPT_14 were the most abundantly expressed
138 at 24 and 72 hpi, respectively (**Figure 4A**). Our analysis of the FPKM values of transcripts per region/TU
139 revealed a similar pattern: the E2 region was the most abundantly expressed at 12 hpi, after which the MLP
140 region assumed dominance (**Figure 4B**).

141 Next, we estimated the relative abundances of all splice junctions at each time point using the raw reads.
142 Only junctions with a read coverage of at least 1% of the total splice junction reads at the given time point
143 were considered significant and included in **Tables 2a-2c**. At 12 hpi, 18 junctions met the 1% threshold,
144 predominantly from early regions (E1, E2, E3, and E4), although the MLTU was the single most predominant
145 region overall, constituting 38.8% of all the junction reads (**Table 2a** and **Supplementary Table S1a**). The
146 most abundant junctions at 12 hpi remained the most significantly expressed at 24 hpi. However, here, the
147 MLP-derived junctions unsurprisingly became even more predominant overall, accounting for 45.7% of all
148 the junction reads counted (**Table 2b** and **Supplementary Table S1b**). At 72 hpi, the trend of increased
149 activity of the MLP continued as expected; at this time, the MLP region junctions were not only the most
150 abundant overall — accounting for 67.3% of all junction reads, — but also contained the most significantly
151 expressed individual junctions (**Table 2c**, **Supplementary Table S1c** and **Figure 4C**). When we limited this
152 analysis to only junctions in the final transcriptome, we observed the relative abundances of the junctions for
153 each region over time to be similar to the pattern seen with all the junctions included (**Figure 4D**).

154 Finally, we analyzed splice donor and acceptor site nucleotide usage over time to investigate any peculiarities
155 that THEV may exhibit, generally or over the course of the infection. We found that most splice donor-acceptor
156 sequences were, unsurprisingly, the canonical GU-AG nucleotides. However, the splice acceptor-donor
157 pairing became less specific over time, such that all combinations of nucleotide pairs were eventually detected
158 (**Figure 5**).

159 **Early Region 1 (E1) transcripts**

160 In MAdVs, E1 is the first region transcribed post-viral DNA entry into the host cell nucleus, mediated solely
161 by host transcription machinery (18). Translated E1 proteins subsequently activate other viral promoters in
162 conjunction with host transcription factors (10). Despite subdivision into E1a and E1b units in MAdVs, our
163 THEV data does not reflect this. This region is predicted to encode only two ORFs: ORF1 (sialidase) and
164 Hyd (a hydrophobic product with unknown function) in THEV.

165 We identified four novel transcripts in this region, containing 3 unique splice junctions (**Figure 6**), and
166 encoding four distinct novel ORFs in addition to Hyd. All transcripts have coding potential (CP) for the Hyd
167 protein as the 3'-most coding sequence if secondary start codon usage is considered (17, 18). Also, all
168 the transcripts have a common transcription termination site (TTS; at position 2325 bp), but TRXPT_1 and
169 TRXPT_2 have an upstream transcription start sites (TSS) to TRXPT_3 and TRXPT_4. Given that E1
170 mRNAs in MAdVs share a common TTS and TSS, differing only in the internal splicing (18), we consider
171 the upstream TSS (position 54 bp) as the actual TSS for all E1 region transcripts. We also identified the
172 canonical polyadenylation signal (PAS; AAUAAA) in the immediate context of the TTS at position 2323 bp
173 (location of the “U” in the PAS sequence); see **Supplementary Table S2**.

174 From the 5'-most start codon (SC), TRXPT_1 encodes a multi-exonic novel 17.9 kDa, 160 residue protein
175 (ORF9). TRXPT_2 encodes a two-exon 66.4 kDa, 597 residue novel protein (ORF10), spanning almost the
176 entire predicted ORF1 and Hyd. The intron of TRXPT_2 excludes the C-terminus of ORF1 (including its
177 stop codon) from ORF10 but the SC of ORF10 is 102 bp upstream and in-frame with the predicted SC of
178 ORF1. TRXPT_3, similar to TRXPT_1 but lacking the second exon, encodes a 13.1 kDa, 115 residue protein
179 (ORF4), previously predicted (27) but excluded in later annotations (1, 12). Our data suggest it is genuinely
180 expressed. Lastly, TRXPT_4 encodes a distinct novel 15.9 kDa, 143 residue protein (ORF11).

181 The splice junctions of all transcripts in this region, except for TRXPT_4, were validated by cloning of viral
182 cDNA and Sanger sequencing (see **Supplementary PCR methods**). During TRXPT_2 validation, ORF1
183 was found on the agarose gel (an unspliced band size) and Sanger sequencing results showed it to be a
184 transcribed mRNA (**Supplementary PCR methods**). This was corroborated by our 3' RACE experiment,
185 which showed a transcript (TRXPT_2B) spanning the entire ORF1 and Hyd ORFs without splicing, with a
186 poly-A tail immediately after the E1 TTS. The 5'-most coding sequence (CDS) of this transcript (TRXPT_2B)
187 encodes ORF1. However, TRXPT_2B has an upstream and in-frame SC to the predicted SC of ORF1,
188 suggesting that the predicted ORF1 CDS is truncated – the expressed ORF1 (eORF1) shares the same SC
189 as ORF10, but has a unique stop codon (STC). See **Supplementary Table S3** for all transcripts and their
190 encoded proteins.

191 **Early Region 2 (E2) and Intermediate Region (IM) transcripts**

192 The E2 TU expressed on the anti-sense strand, is subdivided into E2A and E2B and encodes three classical
193 AdV proteins – pTP and Ad-pol (E2B proteins), and DBP (E2A protein) – essential for genome replication (17,
194 18). Unlike MAdV where two promoters are known (17), we discovered only a single TSS (E2 TSS; 18,751
195 bp) for both E2A and E2B transcripts in THEV. However, E2A and E2B transcripts have distinct TTSs, with
196 E2B transcripts sharing the TTS of the IVa2 transcript of the IM region similar to MAdVs (17, 18) (**Figure 7**).
197 The E2A ORF, DBP, is one of three THEV ORFs predicted to be spliced from two exons. The corresponding
198 transcript (TRXPT_21) in our data matches the predicted splice junction but includes an additional non-coding
199 exon at the 5'-end (E2-5'UTR). Thus, TRXPT_21 is a three-exon transcript encoding DBP (380 residues,
200 43.3 kDa) precisely. TRXPT_21 was also corroborated in a 3' RACE experiment. Additionally, from the 3'
201 RACE data, we found a splice variant of TRXPT_21 which retains the second intron, leading to a 2-exon
202 transcript (TRXPT_21B). Although longer, TRXPT_21B encodes a truncated isoform of DBP (tDBP; a 346
203 residue, 39.3 kDa product) using a downstream in-frame SC but the same STC as DBP. Both TRXPT_21 and
204 TRXPT_21B share a common TTS, seen in our 3' RACE data, located 39 bp downstream of the CDS in an
205 adenine/thymine (A/T)-rich sequence followed by the poly-A tail sequence, suggesting this position (16,934
206 bp) as the true E2A TTS. There are two canonical PASs (AAUAAA; 16,964 and 16950 bp) immediately after
207 the CDS any of which can serve as the PAS without affecting the encoded proteins (**Supplementary Table**
208 **S2**).

209 The E2B region transcripts also start with the E2-5'UTR but extend downstream to reach the TTS at
210 2334 bp in the IM region, which is in the immediate context of a canonical PAS (position 2333 bp) where
211 polyadenylation likely occurs. The E2B transcripts, TRXPT_6 and TRXPT_7, are almost identical except
212 for an extra splice junction at the 3'-end of TRXPT_6 (**Figure 7**). TRXPT_7 has the CP for both classical
213 proteins (pTP and Ad-pol) encoded in this region, with the pTP ORF predicted to be spliced from two exons.
214 The predicted splice junction of pTP is corroborated by our data but the full transcript is markedly longer
215 than the predicted ORF, although the encoded product (pTP) remains unchanged. Ad-pol (polymerase) is
216 encoded downstream of pTP with secondary start codon (secSC) usage. The CP of TRXPT_6 slightly differs
217 from TRXPT_7 because a new STC resulting from the extra splice site forms a minimal truncation of the
218 Ad-pol encoded from its secSC.

219 While both TRXPT_6 and TRXPT_7 have the CP for Ad-pol with secSC usage, in all AdVs studied, the
220 two proteins (pTP and Ad-pol) are encoded by separate mRNAs with identical first three 5' exons and TTS,
221 but different splice junctions to the terminal coding exons. Hence, we checked for a longer splice junction
222 between the third and fourth (terminal) exons of TRXPT_7 with our junction validation method (targeted PCR,

cloning, and Sanger sequencing). We discovered a unique splice junction (10,981-7062 bp) not present in our RNA-seq data. If initiated from the E2 TSS and terminated at the E2B TTS, this transcript (TRXPT_31) would encode Ad-pol in its 5'-most CDS (**Figure 7**).

Our RNA-seq data also showed a novel short transcript (TRXPT_15) entirely nested within the terminal exon of TRXPT_7 but with a unique splice site. This transcript is an incomplete construction from the mapped reads as it contains a truncated CDS. However, we validated this splice junction to be genuine (**Supplementary PCR methods**).

The IM region is a single-transcript TU, encoding a single classical protein, IVa2. The promoter expressing this single transcript (TRXPT_5) is embedded in the E2B region and shares a TTS with E2B transcripts (17, 18). TRXPT_5 is a two-exon transcript with a non-coding first exon, except the last 2 nucleotides, which connect with the first nucleotide of the second exon to form the 5'-most SC. This new SC is four codons upstream and in-frame of the predicted IVa2 SC. Beside the four additional N-terminus residues, the protein sequence is unchanged.

Early Region 3 (E3) transcripts

The E3 region, nested within the MLTU, encodes proteins that modulate and evade host immune defenses. In MAdVs, this region contains seven ORFs expressed from multiple transcripts sharing the same TSS (from the E3 promoter) but having different TTSs (10, 17, 18). However, some E3 transcripts use the TSS of the MLP. Due to sharing the same TSS, in MAdVs, secSC usage is heavily relied on for gene expression in this region as utilizing only the first SC cannot produce the downstream proteins in this TU. The 12.5K ORF and transcripts using the MLP TSS are exceptions (17).

In THEV, only one ORF (E3) was predicted in this region. However, as the E3 TU is nested in the MLTU, transcripts from the L4 promoter (100K, 22K, 33K, and pVIII) overlap the E3 region transcripts entirely and share similar TSS and TTS locations (**Figure 8**). Therefore, we have categorized these two groups together as E3 transcripts.

We identified seven novel transcripts (TRXPT_22, TRXPT_23, TRXPT_24, TRXPT_25, TRXPT_26, TRXPT_27, TRXPT_29) from our RNA-seq data, all originating from two distinct TSSs. We consider the first TSS (position 18,230 bp) as corresponding to the L4 promoter (L4P) and the other at 18,727 bp as corresponding to the E3 promoter (E3P). We also identified the canonical or other known PAs (28) near the TTS of the transcripts (see **Supplementary Table S2**). These E3 transcripts collectively have the CP for several predicted THEV ORFs: 100K, 22K, 33K, pVIII, and E3, as well as Fiber (IV) and ORF7 of the MLTU (see **Supplementary Table S3**). However, some of these CDSs differ from the predictions due to

either unknown exons or the presence of an in-frame upstream SC. For instance, we discovered that 33K, predicted to be spliced from two exons, is actually a significantly longer four-exon ORF (e33K; 19.8 kDa, 171 residues) encoded on TRXPT_24. Its first two exons were unknown but the last two match the predicted exons and the CDS is in-frame, albeit the first 20 bp of the predicted 33K (including the SC) is spliced out as part of the second intron of TRXPT_24. TRXPT_24 also has the CP for pVIII and E3 if we consider downstream SC usage. However, we found an upstream in-frame SC for the predicted E3; thus, this longer version of E3 (eE3) is likely the genuinely expressed ORF. TRXPT_29, the shortest transcript in this TU, encodes a novel 73 residue protein (8.3KI) across its two exons using the SC of e33K with a unique STC. TRXPT_23, spliced identically as TRXPT_29, also encodes 8.3KI from its first SC. Similarly, TRXPT_22 encodes a 73 residue novel protein (8.3KII) from its first SC that shares over 80% similarity with 8.3KI, but they differ at the C-terminus. Considering downstream SC usage, both TRXPT_22 and TRXPT_23 can encode pVIII and eE3 in that order, but TRXPT_23 being longer, also has the CP for the Fiber ORF.

As the splice junctions of TRXPT_22, TRXPT_23, TRXPT_24, and TRXPT_29 share the same genomic space, their validation was done with a single primer pair, and they were differentiated from each other by cloning the cDNA and Sanger sequencing (**Supplementary PCR methods**). In addition to corroborating the splice junctions for the aforementioned transcripts, the Sanger sequencing results also showed a distinct splice variant undetected in our RNA-seq transcriptome. This was a three-exon transcript (TRXPT_30) with identical first and last exons as TRXPT_23, which also contained the second exon of TRXPT_24 (**Figure 8**). TRXPT_30 encodes a novel 140 residue, 15.7kDa protein (e22K), spanning all three exons. Interestingly, the last 81 C-terminus residues of e22K are identical to 22K (89 residues), a single-exon ORF predicted to use the same SC as 33K. Just as seen for 33K, the first 20 bp of 22K is intronic, excluding the first 7 residues of 22K from e22K. We consider e22K as a long variant of the predicted 22K ORF. Assuming TRXPT_30 shares the same TSS and TTS as TRXPT_23, it would also have the downstream CP of TRXPT_23.

TRXPT_25, the largest transcript in the TU, is a two-exon transcript, encoding a novel protein (t100K; 543 residues), which is a shorter isoform of the predicted 100K ORF. secSC usage on this transcript yields the predicted 22K ORF. It also has the CP for pVIII and eE3 downstream. Furthermore, during the validation of the TRXPT_25 splice junction using primers that span its junction (18,350-18,717 bp), we noticed a DNA band corresponding to the full unspliced sequence (**Supplementary PCR methods**). As TRXPT_25 only falls short of encoding the complete predicted 100K protein due to its splice junction, this band (which we cloned and validated by Sanger sequencing) suggests that the predicted 100K is indeed expressed. We assume that this transcript (TRXPT_25B) shares the same TSS and TTS as TRXPT_25.

Lastly, TRXPT_26 and TRXPT_27, both originate from the E3P but have distinct TTSs. TRXPT_26 encodes

286 pVIII as the 5'-most ORF and has the CP for eE3 and Fiber in that order. TRXPT_27, a two-exon transcript,
287 encodes Fiber as the 5'-most ORF, and ORF7 downstream with secSC usage. TRXPT_13 is an L4P
288 transcript that uses the MLP TSS; it is discussed under the MLTU transcripts.

289 **Early Region 4 (E4) transcripts** This TU is found at the 3'-end of the genome and expressed on the
290 anti-sense strand. Based on nucleotide position, ORF7 and ORF8 were predicted in this region (1); however,
291 as ORF7 is neither on the anti-sense strand nor transcribed from a promoter in the E4 region, we only
292 classify ORF8 in this TU. This is corroborated by our RNA-seq data, showing only one transcript in this
293 region on the anti-sense strand (**Figure 9**). The transcript (TRXPT_28) spans 25192-26247 bp and is spliced
294 at 25701-26055 bp, forming a two-exon transcript. The second exon fully matches the predicted ORF8 with
295 12 extra base pairs at the 3'-end. However, we identified a SC 192 bp upstream of the predicted SC in the
296 first exon from which an in-frame protein is encoded. We consider this longer isoform (eORF8 – 26.4 kDa,
297 229 residues) as the genuinely expressed ORF. We also identified a canonical PAS 11 bp upstream of TTS
298 (**Supplementary Table S2**).

299 **Major Late Transcription Unit (MLTU) or MLP Region transcripts**

300 The MLTU transcripts, dominant in the late phase of the AdV infectious cycle, are produced by alternative
301 polyadenylation and splicing of a primary transcript and grouped into five transcript classes (L1-L5). About
302 13 out of the 23 predicted ORFs in THEV fall within this TU, some of which we have categorized under the
303 E3 TU instead. Our RNA-seq data revealed 12 transcripts (TRXPT_8, TRXPT_9, TRXPT_10, TRXPT_11,
304 TRXPT_12, TRXPT_13, TRXPT_14, TRXPT_16, TRXPT_17, TRXPT_18, TRXPT_19, TRXPT_20) in this
305 TU, most of which have the 5' TPL sequence as in all AdVs. However, three transcripts (TRXPT_16,
306 TRXPT_17, TRXPT_18) use a different leader sequence (sTPL), where a different first exon is used instead
307 of the first TPL exon, and TRXPT_20 uses only the third TPL exon (TPL3); see **Figure 10**.

308 We identified five TTSs (10,549, 12,709, 16,870, 22,116, 25,168 bp) in this TU, which we consider as
309 corresponding to the five late mRNA classes (L1-L5), respectively. L1 mRNAs include TRXPT_8, encoding
310 the 52K ORF as predicted. L2 mRNAs include TRXPT_16, TRXPT_17, and TRXPT_18, all containing the
311 sTPL with their respective coding exons. They encode pIIa, III (penton), and pVII, respectively. The L3
312 mRNAs, TRXPT_14 and TRXPT_20, both encode the hexon (II) ORF but hexon is the only ORF encoded on
313 TRXPT_14, whereas TRXPT_20 encodes pX (pre-Mu), pVI, and hexon in that order. L4 mRNAs, TRXPT_9,
314 TRXPT_10, TRXPT_11, and TRXPT_13 are the largest transcripts in the transcriptome and encode several
315 similar late proteins. TRXPT_9 and TRXPT_10 are very similar but not identical. The last exon of TRXPT_9
316 seems to be truncated and likely shares the same TTS as TRXPT_10. They both encode pVII as the 5'-most
317 ORF and also have the CP for pX, pVI, hexon, a longer variant of protease (eProt) from an upstream in-frame

318 SC, and ORF12 (a novel 120 residue protein). Additionally, they have the CP for pVIII and eE3. TRXPT_11
319 encodes hexon as its 5'-most ORF and also has the CP for eProt, ORF12, e33K, pVIII and eE3. Typically,
320 MLTU transcripts splice the TPL onto a splice site just upstream of the ORF to be expressed (17). While
321 this holds true for most MLTU ORFs, several late ORFs (pVI, protease, and ORF7) do not have such close
322 proximity splicing but are contained in larger transcripts such as these L4 mRNAs, strongly suggesting the
323 use of non-standard ribosomal initiation mechanisms such as secSC usage or ribosome shunting described
324 in other AdVs for their translation (17, 29). TRXPT_13, an E3 ORF utilizing the MLP TSS, encodes the
325 classical L4P genes, pVIII and eE3. Lastly, the L5 class transcript, TRXPT_12, encodes Fiber as its 5'-most
326 ORF but also has the CP for ORF7. Interestingly, the CP of TRXPT_12 and TRXPT_27 of the E3 TU are
327 identical but are initiated from different TSSs.

328 **DISCUSSION**

329 While the advent of next-generation sequencing has rendered easier the study of large and complex eukary-
330 otic transcriptomes, studying the smaller, compact viral transcriptomes remains unintuitively challenging,
331 as the transcripts typically have significant overlaps due to genome economization. AdV transcriptomes
332 escalate the difficulty due to the wide array of mRNAs produced via very complex alternative splicing and
333 polyadenylation, all initiated from relatively few promoters. Standard RNA-seq analysis programs, not primar-
334 ily designed for such compact, gene-dense, and complex transcriptomes, further compound this challenge.
335 Furthermore, in our case, no prior transcriptomic studies for THEV exist. Our approach combines standard
336 RNA-seq analysis programs with custom analyses and experimentally validating all splice junctions with
337 independent methods. The transcript map for THEV produced from our analysis is strikingly similar to that of
338 the MAdVs.

339 Our work provides the first insights into THEV splicing, revealing 34 transcripts grouped into five transcription
340 units (TUs). The general temporal gene expression regulation observed in MAdVs, with early regions peaking
341 at earlier time points followed by MLTU predominance at later time points, seems to also apply to THEV.
342 An unexpected observation is that the pileup of mapped reads to THEV seems consistently skewed over
343 similar regions of the genome at all time points. Given the temporal regulation of AdVs gene expression, we
344 anticipated distinct differences in read pileups over the genome at different time points, indicating the different
345 stages of infection. This may be due to an unsynchronized infection, leading to transcripts overlapping the
346 time points. Further research is required to determine the precise temporal regulation of THEV.

347 Short read deep sequencing effectively reconstructs full AdV mRNA structures, particularly mapping splice
348 sites (18). However, the substantial overlapping nature of AdV mRNAs and fragmentation during library
349 preparation make it challenging to map the exact TSS, TTS, and PASs of assembled transcripts. Also,
350 transcripts with significant overlaps may be assembled as a single, longer mRNA, since the short reads
351 alone do not provide enough context for the transcript assembler (StringTie) to distinguish them. Our results
352 show transcripts in the same TU initiating or terminating in similar areas, but not at the exact same position.
353 We consider the most upstream TSS or most downstream TTS for the transcripts involved but we present
354 them unchanged in all the figures shown (see **Supplementary Table S2**). Also, comparing our results to the
355 better-studied MAdV transcriptomes, we believe some long transcripts in the MLTU (TRXPT_9, TRXPT_10,
356 and TRXPT_11) are likely due to fusing some E3 transcripts to the terminal exons of the MLTU transcripts by
357 StringTie, making them significantly longer. These mRNAs have unusually many exons and their last few
358 exons are identical to some E3 mRNAs. Future studies using long read sequencing technologies will provide
359 more precise mapping of the TSS and TTS and clarify the structures of the long MLTU transcripts.

360 While most predicted ORFs are encoded by the spliced transcripts, we found some that seem to be truncated
361 predictions, as either an upstream in-frame SC or unknown upstream exons were found. Other ORFs were
362 identified that were either shorter or longer isoforms of some predicted ORF. We also found several novel
363 unpredicted ORFs (**Supplementary Table S3**). On this basis, we anticipate that further studies will likely
364 reveal more unpredicted novel ORFs or new variants of predicted ORFs. Furthermore, it is not unreasonable
365 to presume that several splice variants will likely be found as evidenced firstly by finding unique transcripts
366 using 3' RACE and during our splice junction validation steps. And secondly, recent studies (17, 18, 22) are
367 still discovering novel mRNA variants for even the best studied MAdVs decades later.

368 Eukaryotic mRNAs are typically functionally monocistronic, with the 5'-most AUG determining the translation
369 reading frame. However, AdV mRNAs, which span more than one ORF, are functionally polycistronic,
370 employing non-standard mechanisms of translation initiation such as secSC usage and ribosome shunting
371 (10, 22). AdVs use secondary AUGs as initiation codons for most E1b proteins and some E3 proteins. In
372 fact, recent studies show that secSC usage is found transcriptome-wide. This is thought to occur because
373 translation initiation at the first SC is inefficient, allowing downstream SCs to be employed (17). Ribosomal
374 shunting or jumping mechanism is utilized for MLTU transcripts that have the TPL. This mechanism allows the
375 ribosome to translocate to a downstream AUG, under the direction of the shunting elements in the TPL, even
376 if a start codon in a good Kozak sequence context is bypassed. Thus, predicting the protein(s) expressed
377 from an AdV mRNA is uncertain as any one of the AUGs may be selected (10, 22). Almost all the THEV
378 transcripts in our data have the CP for several ORFs, some spanning as many as six ORFs. This supports
379 the usage of these special ribosome initiation mechanisms as several predicted and novel ORFs found on
380 mRNA in our data could not be translated using only the typical ribosome scanning mechanism. Interestingly,
381 several distinct THEV mRNAs have identical CPs. This is also observed in human AdVs in a recent study
382 (17). They proposed that this may permit protein production to be fine-tuned through alteration in the balance
383 between different mRNA groups expressing that ORF.

384 AdV alternative splicing undergoes a regulated temporal shift in splice site usage, previously thought to be
385 limited to certain TUs. However, recent studies suggest that AdVs routinely produce different combinations
386 of splice acceptor–donor pairs across all TUs (10, 17, 22, 30). The details of this phenomenon have been
387 best studied for the E1A and L1 units. AdVs modulate the activities of the splicing factor U2AF and the
388 cellular SR family of splicing factors (reviewed here (30)), and encode several proteins that influence the RNA
389 splice site used. This phenomenon appears to occur in the THEV transcriptome, as the stringency of splice
390 acceptor-donor pairs selected decreases from the onset of the late phase (**Figure 5**). Recent studies show
391 that a virtually unlimited number of combinatorial alternative splicing events occur in an AdV lytic infection,

392 resulting in a variety of novel transcripts (17, 22). It is unlikely that the entire repertoire of mRNA produced via
393 this mechanism will actually be translated. However, it has been speculated that the plasticity in alternative
394 RNA splicing enables AdVs to fine-tune protein synthesis by providing different alternatively spliced variants
395 encoding the same protein under changing conditions, conferring an evolutionary advantage (17, 22).

396 In summary, the THEV transcriptome bears remarkable similarity to the better-studied MAdVs. The tran-
397 scriptome is organized into five TUs, with temporal regulation divided into early and late genes, and a
398 broad repertoire of transcripts are produced via virtually unlimited alternative splicing. However, the THEV
399 transcriptome appears less sophisticated (i.e, it encodes fewer genes) than MAdVs, primarily because the
400 MAdV genomes are close to twice as long as that of THEV. The lack of subdivision of the E1 region into E1a
401 and E1b is one of the most obvious examples. Also, the MAdV E4 region encodes several proteins unlike
402 in THEV where only one transcript encoding one protein was found. The complexity of the MLTU leader
403 sequences is another example. While the majority of the THEV MLTU transcripts begin with the TPL just like
404 MAdVs with a small subset using a variant leader sequence (sTPL), significantly more diverse 5'-UTRs are
405 employed for MAdV MLTU transcripts. Namely, the TPL, the so-called x, y, and z leaders, and the i-leader
406 are 5' leaders utilized by MAdV MLTU mRNAs. The absence of these non-TPL leaders in our data could
407 mean that the 5'-UTR diversity of THEV's MLTU mRNAs is more limited due to its smaller genome size or
408 future studies using long read sequencing technologies could uncover more variety not seen in our results.

409 **METHODS**

410 **Cell culture and THEV Infection**

411 The Turkey B-cell line (MDTC-RP19, ATCC CRL-8135) was grown as suspension cultures in 1:1 complete
412 Leibovitz's L-15/McCoy's 5A medium with 10% fetal bovine serum (FBS), 20% chicken serum (ChS), 5%
413 tryptose phosphate broth (TPB), and 1% antibiotic solution (100 U/mL Penicillin and 100 μ g/mL Streptomycin),
414 at 41°C in a humidified atmosphere with 5% CO₂. Infected cells were maintained in 1:1 serum-reduced
415 Leibovitz's L15/McCoy's 5A media (SRLM) with 2.5% FBS, 5% ChS, 1.2% TPB, and 1% antibiotic solution. A
416 commercially available THEV vaccine was purchased from Hygieia Biological Labs as a source of THEV-A
417 (VAS strain). The stock virus was titrated using an in-house qPCR assay with titer expressed as genome
418 copy number (GCN)/mL, similar to Mahshoub *et al* (31) with modifications. Cells were infected in triplicate
419 at a multiplicity of infection (MOI) of 100 GCN/cell, incubated at 41°C for 1 hour, and washed three times
420 with phosphate buffered saline (PBS) to get rid of free virus particles. Triplicate samples were harvested at
421 4-, 12-, 24-, and 72-hpi for total RNA extraction. The infection was repeated but samples in triplicate were
422 harvested at 12-, 24-, 36-, 48-, and 72-hpi for PCR validation of novel splice sites. Still one more independent
423 infection was done at time points ranging from 12 to 168-hpi for qPCR quantification of virus titers.

424 **RNA extraction and Sequencing**

425 Total RNA was extracted from infected cells using the Thermo Fisher RNAqueous™-4PCR Total RNA Isolation
426 Kit (which includes a DNase I digestion step) per manufacturer's instructions. An agarose gel electrophoresis
427 was performed to check RNA integrity. The RNA quantity and purity was initially assessed using nanodrop,
428 and RNA was used only if the A260/A280 ratio was 2.0 ± 0.05 and the A260/A230 ratio was >2 and <2.2.
429 Extracted total RNA samples were sent to LC Sciences, Houston TX for poly-A-tailed mRNA sequencing
430 where RNA integrity was checked with Agilent Technologies 2100 Bioanalyzer High Sensitivity DNA Chip
431 and poly(A) RNA-seq library was prepared following Illumina's TruSeq-stranded-mRNA sample preparation
432 protocol. Paired-end sequencing to generate 150 bp reads was performed on the Illumina NovaSeq 6000
433 sequencing system.

434 **Validation of Novel Splice Junctions**

435 All splice junctions identified in this work are novel except one predicted splice site each for pTP, DBP,
436 and 33K, which were corroborated in our work. However, these predicted splice junctions had not been
437 experimentally validated hitherto, and we identified additional novel exons, giving the complete picture of

438 these transcripts. The novel splice junctions discovered in this work using the StringTie transcript assembler
439 were validated by PCR, cloning, and Sanger Sequencing (**Supplementary PCR methods**). Briefly, primers
440 spanning a range of novel exon-exon boundaries for each specific transcript in a transcription unit (TU) were
441 designed. Universal forward or reverse primers for each respective TU were designed and paired with primers
442 binding specific positions in each transcript. Each forward primer contained a KpnI restriction site and each
443 reverse primer, an XbaI site in the primer 5' ends. After first-strand cDNA synthesis of total RNA obtained
444 from THEV infected MDTC-RP19 cells was done using SuperScript™ IV First-Strand Synthesis System, the
445 primers were used in a targeted PCR amplification, the products analyzed with agarose gel electrophoresis
446 to confirm expected band sizes, cloned by traditional restriction enzyme method, and Sanger sequenced
447 to validate these splice junctions at the sequence level. The total RNA was extracted as described above,
448 including the DNase I digestion step. We included infected total RNA controls with no reverse transcriptase
449 (no RT) during the cDNA synthesis step and the parent RNA were digested using RNase H after cDNA
450 synthesis was complete to ensure that the bands obtained from the targeted PCR amplifications did not
451 originate from the viral genomic DNA. As seen in the agarose gel images in **Supplementary PCR methods**,
452 DNA bands were not found in the “no RT” controls, indicating that the DNA bands seen are of cDNA origin.

453 **3' Rapid Amplification of cDNA Ends (3' RACE)**

454 A rapid amplification of sequences from the 3' ends of mRNAs (3' RACE) experiment was performed using
455 a portion of the extracted total RNA of infected MDTC-RP19 cells used for the RNA-seq experiment as
456 explained above. We followed the protocol described by Green *et al* (32) with modifications. Briefly, 1 μ g of
457 total RNA was reverse transcribed to cDNA using SuperScript™ IV First-Strand Synthesis System following
458 the manufacturing instructions using an adapter-primer with a 3'-end poly(T) and a 5'-end BamHI restriction
459 site. A gene-specific sense primer with a 5'-end KpnI restriction site paired with an anti-sense adapter-primer
460 with a 5'-end BamHI site were used to amplify target sections of the cDNA using Invitrogen's Platinum™ Taq
461 DNA polymerase High Fidelity, following manufacturer's instructions. The PCR amplicons were restriction
462 digested, cloned, and Sanger sequenced.

463 **Computational Analysis of RNA Sequencing Data: Mapping and Transcript characterization**

464 Sequencing reads were analyzed following a well-established protocol described by Pertea *et al* (25), using
465 Snakemake - version 7.24.0 (33), a popular workflow management system to drive the pipeline. Briefly,
466 sequencing reads were trimmed with the Trim-galore - version 0.6.6 (34) program to achieve an overall Mean
467 Sequence Quality (Phred Score) of 36. Trimmed reads were mapped simultaneously to the complete genomic

468 sequence of avirulent turkey hemorrhagic enteritis virus (<https://www.ncbi.nlm.nih.gov/nuccore/AY849321.1/>)
469 and *Meleagris gallopavo* (<https://www.ncbi.nlm.nih.gov/genome/?term=Meleagris+gallopavo>) using Hisat2
470 - version 2.2.1 (25) with default settings. The generated binary alignment (BAM) files from each infection
471 time point were filtered for reads mapping to the THEV genome using Samtools - version 1.16.1 and fed into
472 StringTie - version 2.2.1 (25) to assemble the transcripts, using a gene transfer format (GTF) annotation
473 file derived from a gene feature format 3 (GFF3) annotation file obtained from NCBI, which contains the
474 predicted ORFs of THEV as a guide. GFFCOMPARE - version 0.12.6 was used to merge all transcripts
475 from all time points without redundancy and using a custom R script, adenovirus transcripts units (regions)
476 were assigned to each transcript, generating the transcriptome of THEV. StringTie was set to expression
477 estimation mode to calculate FPKM scores for all transcripts after which Ballgown - version 2.33.0 in R was
478 used to perform the statistical analysis on the transcript expression levels. Samtools was also used to count
479 the total sequencing reads for all replicates at each time point and Regtools - version 1.0.0 was used to
480 count all junctions, the reads supporting them, and extract all other information related to the junction. See
481 **Supplementary Computational Analysis** for the details of transcript expression level estimations and splice
482 junction read counts.

483 DATA AVAILABILITY

484 The raw sequencing read data (FastQ), transcript expression counts, and total unique junctions have
485 been deposited at the National Center for Biotechnology Information Gene Expression Omnibus (<http://www.ncbi.nlm.nih.gov/geo>) under accession number GSE254416.
486
487 Data is also available on request by contacting the designated corresponding author.

488 CODE AVAILABILITY

489 All the code/scripts in the entire analysis pipeline are available on github (https://github.com/Abraham-Quaye/thev_transcriptome)

491 ACKNOWLEDGMENTS

492 We thank the Office of Research Computing at Brigham Young University for granting us access to the high
493 performance computing systems to perform the memory-intensive steps in the analysis pipeline of this work.

494 **REFERENCES**

- 495 1. Davison A, Benko M, Harrach B. 2003. Genetic content and evolution of adenoviruses. *The Journal of general virology* 84:2895–908.
- 496 2. Harrach B. 2008. Adenoviruses: General features, p. 1–9. *In* Mahy, BWJ, Van Regenmortel, MHV (eds.), *Encyclopedia of virology* (third edition). Book Section. Academic Press, Oxford.
- 497 3. Upton C, Slack S, Hunter AL, Ehlers A, Roper RL. 2003. Poxvirus orthologous clusters: Toward defining the minimum essential poxvirus genome. *Journal of virology* 77:7590–7600.
- 498 4. McGeoch D, Davison AJ. 1999. Chapter 17 - the molecular evolutionary history of the herpesviruses, p. 441–465. *In* Domingo, E, Webster, R, Holland, J (eds.), *Origin and evolution of viruses*. Book Section. Academic Press, London.
- 499 5. Harrach B, Benko M, Both GW, Brown M, Davison AJ, Echavarría M, Hess M, Jones M, Kajon A, Lehmkühl HD, Mautner V, Mittal S, Wadell G. 2011. Family adenoviridae. *Virus Taxonomy: 9th Report of the International Committee on Taxonomy of Viruses* 125–141.
- 500 6. Kovács ER, Benkő M. 2011. Complete sequence of raptor adenovirus 1 confirms the characteristic genome organization of siadenoviruses. *Infection, Genetics and Evolution* 11:1058–1065.
- 501 7. Davison AJ, Wright KM, Harrach B. 2000. DNA sequence of frog adenovirus. *J Gen Virol* 81:2431–2439.
- 502 8. Kovács ER, Jánoska M, Dán Á, Harrach B, Benkő M. 2010. Recognition and partial genome characterization by non-specific DNA amplification and PCR of a new siadenovirus species in a sample originating from parus major, a great tit. *Journal of Virological Methods* 163:262–268.
- 503 9. Katoh H, Ohya K, Kubo M, Murata K, Yanai T, Fukushi H. 2009. A novel budgerigar-adenovirus belonging to group II avian adenovirus of siadenovirus. *Virus Research* 144:294–297.

- 504 10. Guimet D, Hearing P. 2016. 3 - adenovirus replication, p. 59–84. In Curiel, DT (ed.), Adenoviral
vectors for gene therapy (second edition). Book Section. Academic Press, San Diego.
- 505 11. Beach NM. 2006. Characterization of avirulent turkey hemorrhagic enteritis virus: A study of the
molecular basis for variation in virulence and the occurrence of persistent infection. Thesis.
- 506 12. Beach NM, Duncan RB, Larsen CT, Meng XJ, Sriranganathan N, Pierson FW. 2009. Comparison of
12 turkey hemorrhagic enteritis virus isolates allows prediction of genetic factors affecting virulence. J
Gen Virol 90:1978–85.
- 507 13. Gross WB, Moore WE. 1967. Hemorrhagic enteritis of turkeys. Avian Dis 11:296–307.
- 508 14. Rautenschlein S, Sharma JM. 2000. Immunopathogenesis of haemorrhagic enteritis virus (HEV) in
turkeys. Dev Comp Immunol 24:237–46.
- 509 15. Larsen CT, Domermuth CH, Sponenberg DP, Gross WB. 1985. Colibacillosis of turkeys exacerbated
by hemorrhagic enteritis virus. Laboratory studies. Avian Dis 29:729–32.
- 510 16. Dhami K, Gowthaman V, Karthik K, Tiwari R, Sachan S, Kumar MA, Palanivelu M, Malik YS, Singh
RK, Munir M. 2017. Haemorrhagic enteritis of turkeys – current knowledge. Veterinary Quarterly
37:31–42.
- 511 17. Donovan-Banfield I, Turnell AS, Hiscox JA, Leppard KN, Matthews DA. 2020. Deep splicing plasticity
of the human adenovirus type 5 transcriptome drives virus evolution. Communications Biology 3:124.
- 512 18. Zhao H, Chen M, Pettersson U. 2014. A new look at adenovirus splicing. Virology 456-457:329–341.
- 513 19. Wolfrum N, Greber UF. 2013. Adenovirus signalling in entry. Cell Microbiol 15:53–62.
- 514 20. Falvey E, Ziff E. 1983. Sequence arrangement and protein coding capacity of the adenovirus type 2
"i" leader. Journal of Virology 45:185–191.

- 515 21. Morris SJ, Scott GE, Leppard KN. 2010. Adenovirus late-phase infection is controlled by a novel L4 promoter. *Journal of Virology* 84:7096–7104.
- 516 22. Westergren Jakobsson A, Segerman B, Wallerman O, Bergström Lind S, Zhao H, Rubin C-J, Pettersson U, Akusjärvi G. 2021. The human adenovirus 2 transcriptome: An amazing complexity of alternatively spliced mRNAs. *Journal of Virology* 95.
- 517 23. Djebali S, Davis CA, Merkel A, Dobin A, Lassmann T, Mortazavi A, Tanzer A, Lagarde J, Lin W, Schlesinger F, Xue C, Marinov GK, Khatun J, Williams BA, Zaleski C, Rozowsky J, Röder M, Kokocinski F, Abdelhamid RF, Alioto T, Antoshechkin I, Baer MT, Bar NS, Batut P, Bell K, Bell I, Chakrabortty S, Chen X, Chrast J, Curado J, Derrien T, Drenkow J, Dumais E, Dumais J, Duttagupta R, Falconnet E, Fastuca M, Fejes-Toth K, Ferreira P, Foissac S, Fullwood MJ, Gao H, Gonzalez D, Gordon A, Gunawardena H, Howald C, Jha S, Johnson R, Kapranov P, King B, Kingswood C, Luo OJ, Park E, Persaud K, Preall JB, Ribeca P, Risk B, Robyr D, Sammeth M, Schaffer L, See L-H, Shahab A, Skancke J, Suzuki AM, Takahashi H, Tilgner H, Trout D, Walters N, Wang H, Wrobel J, Yu Y, Ruan X, Hayashizaki Y, Harrow J, Gerstein M, Hubbard T, Reymond A, Antonarakis SE, Hannon G, Giddings MC, Ruan Y, Wold B, Carninci P, Guigó R, Gingeras TR. 2012. Landscape of transcription in human cells. *Nature* 489:101–108.
- 518 24. Aboezz Z, Mahsoub H, El-Bagoury G, Pierson F. 2019. In vitro growth kinetics and gene expression analysis of the turkey adenovirus 3, a siadenovirus. *Virus Research* 263:47–54.
- 519 25. Pertea M, Kim D, Pertea GM, Leek JT, Salzberg SL. 2016. Transcript-level expression analysis of RNA-seq experiments with HISAT, StringTie and ballgown. *Nature Protocols* 11:1650–1667.
- 520 26. Jack Fu [Aut], Alyssa C. Frazee [Aut, Cre], Leonardo Collado-Torres [Aut], Andrew E. Jaffe [Aut], Jeffrey T. Leek [Aut, Ths]. 2017. Ballgown. Bioconductor.
- 521 27. Pitcovski J, Mualem M, Rei-Koren Z, Krispel S, Shmueli E, Peretz Y, Gutter B, Gallili GE, Michael A, Goldberg D. 1998. The complete DNA sequence and genome organization of the avian adenovirus, hemorrhagic enteritis virus. *Virology* 249:307–315.

- 522 28. Beaudoin E, Freier S, Wyatt JR, Claverie J-M, Gautheret D. 2000. Patterns of variant polyadenylation signal usage in human genes. *Genome Research* 10:1001–1010.
- 523 29. Yueh A, Schneider RJ. 1996. Selective translation initiation by ribosome jumping in adenovirus-infected and heat-shocked cells. *Genes & Development* 10:1557–1567.
- 524 30. Akusjarvi G. 2008. Temporal regulation of adenovirus major late alternative RNA splicing. *Frontiers in Bioscience Volume:5006*.
- 525 31. Mabsoub HM, Evans NP, Beach NM, Yuan L, Zimmerman K, Pierson FW. 2017. Real-time PCR-based infectivity assay for the titration of turkey hemorrhagic enteritis virus, an adenovirus, in live vaccines. *Journal of Virological Methods* 239:42–49.
- 526 32. Green MR, Sambrook J. 2019. Rapid amplification of sequences from the 3' ends of mRNAs: 3'-RACE. *Cold Spring Harbor Protocols* 2019:pdb.prot095216.
- 527 33. Mölder F, Jablonski KP, Letcher B, Hall MB, Tomkins-Tinch CH, Sochat V, Forster J, Lee S, Twardziok SO, Kanitz A, Wilm A, Holtgrewe M, Rahmann S, Nahnsen S, Köster J. 2021. Sustainable data analysis with snakemake. *F1000Research* 10:33.
- 528 34. Krueger F, James F, Ewels P, Afyounian E, Weinstein M, Schuster-Boeckler B, Hulselmans G, Sclamons. 2023. FelixKrueger/TrimGalore: v0.6.10 - add default decompression path. Zenodo.

529 **TABLES AND FIGURES**

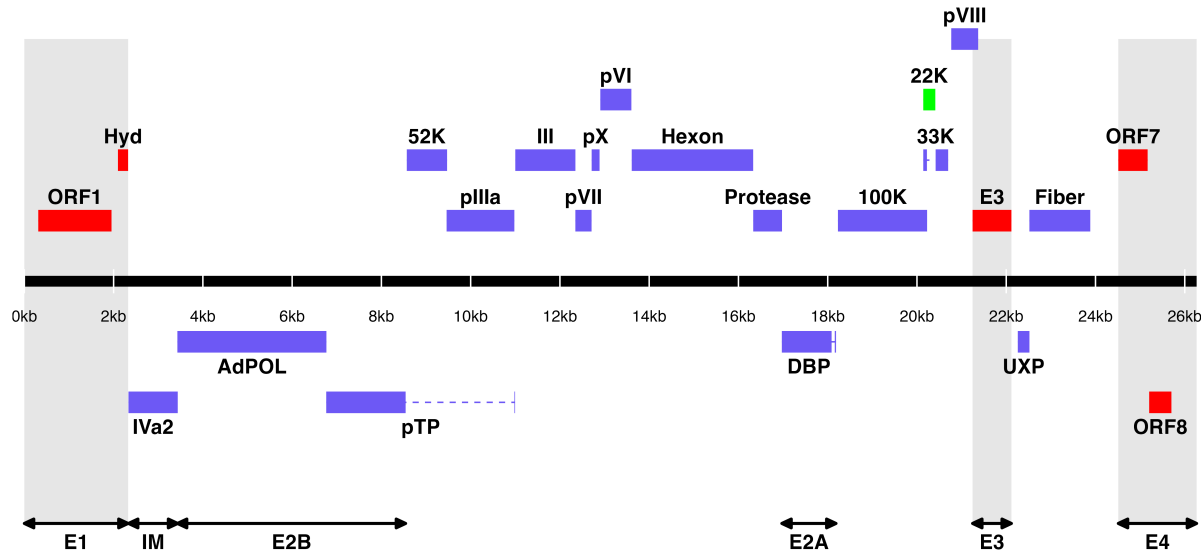
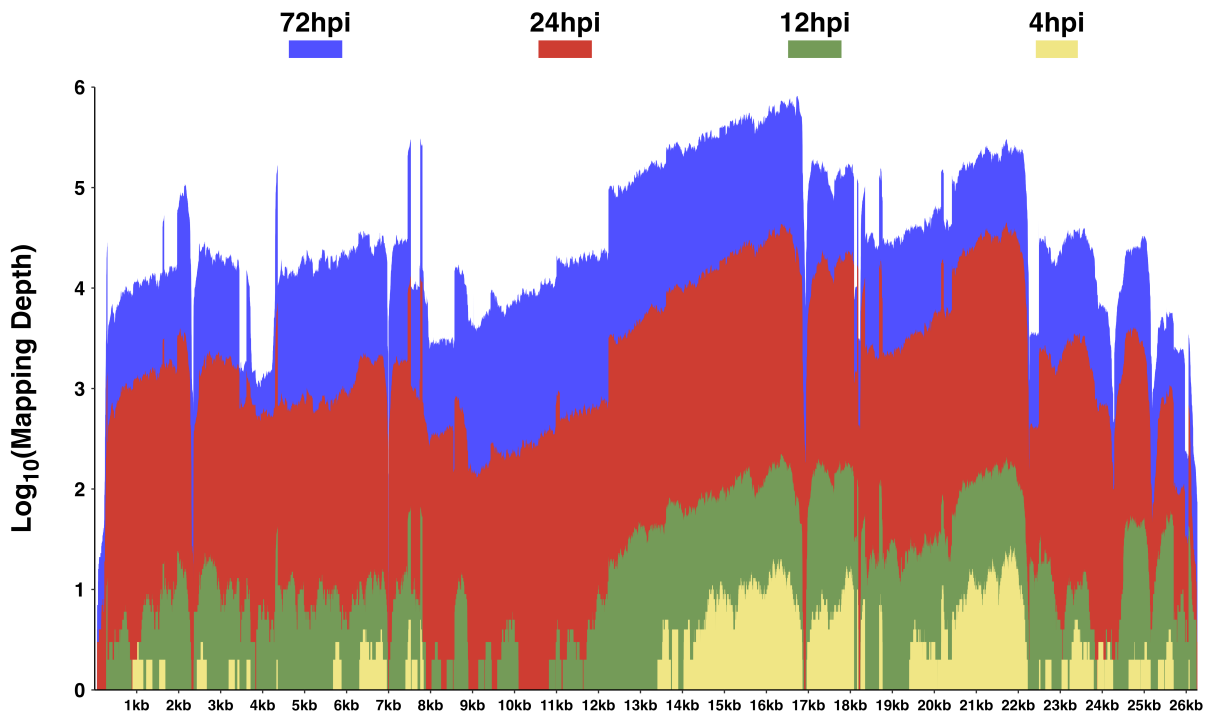


Figure 1. Predicted ORF map of THEV avirulent strain. The central horizontal line represents the double-stranded DNA marked at 2kb intervals as white line breaks. Colored blocks represent viral genes. Blocks above the DNA line are transcribed on the sense DNA strand and those below, on the anti-sense strand. pTP, DBP and 33K are predicted to be spliced and are shown as two exons connected with dashed lines. Shaded regions indicate regions containing “genus-specific” genes (colored red). Genes colored in blue are “genus-common”. The gene colored in light green is conserved in all but Atadenoviruses. Regions comprising the different transcription units are labelled at the bottom (E1, E2A, E2B, E3, E4, and IM); the unlabeled regions comprise the MLTU.

A

Mapping Depth of RNA-seq Reads Over THEV Genome

**B**

THEV Growth Curve in RP-19 Turkey B-Cells

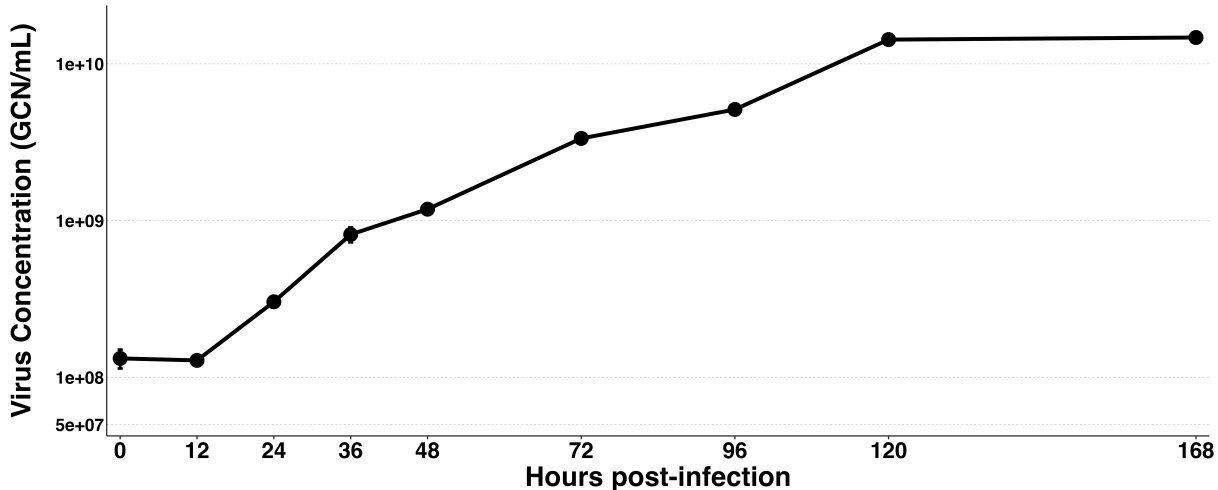


Figure 2: Increasing levels of THEV over time. A) Per base coverage of sequence reads mapping to THEV genome by time point. The pileup of mRNA reads mapping to THEV genome at the base-pair level for each indicated time point. B) Growth curve of THEV (VAS vaccine strain) in MDTC-RP19 cell line. Virus quantities in the freeze-thawed supernatant from infected cells were quantified with a qPCR assay. There is no discernible increase in virus titer up 12 hpi, after which a steady increase in virus titer is measured. The virus titer expands exponentially beginning from 48 hpi, increasing by orders of magnitude before reaching a plateau at 120 hpi. GCN: genome copy number.

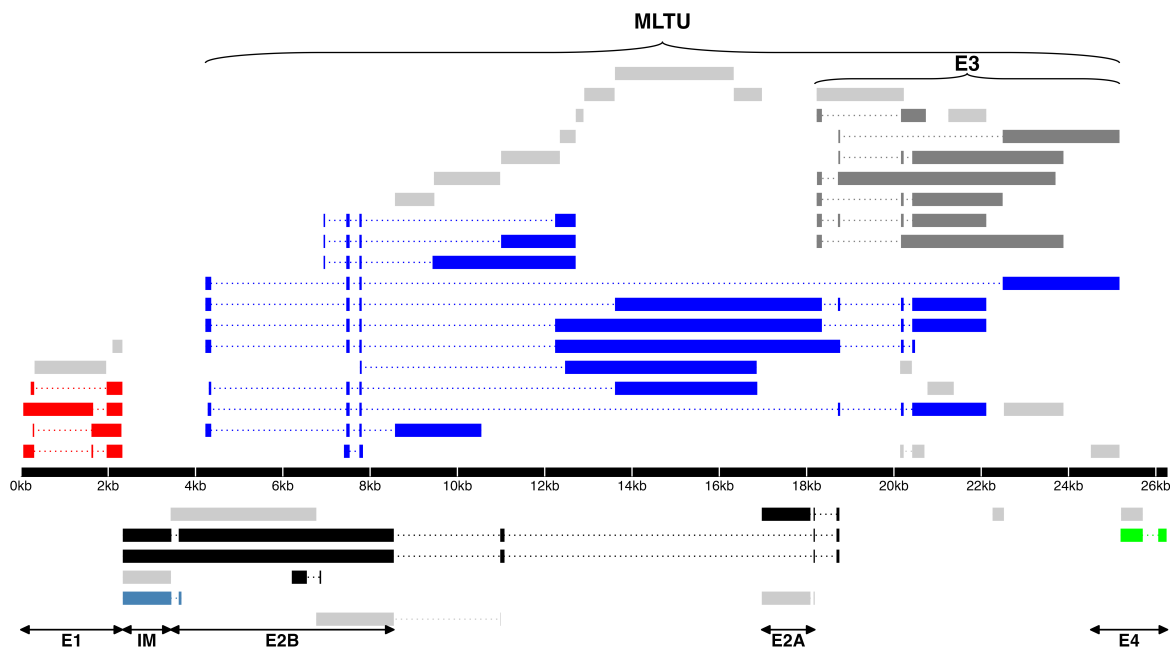
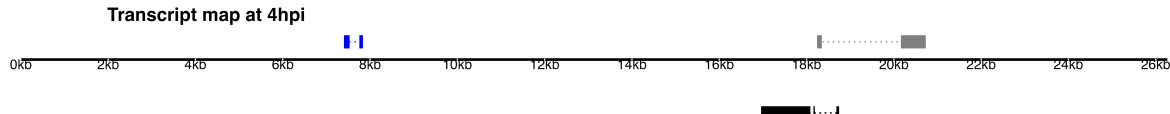
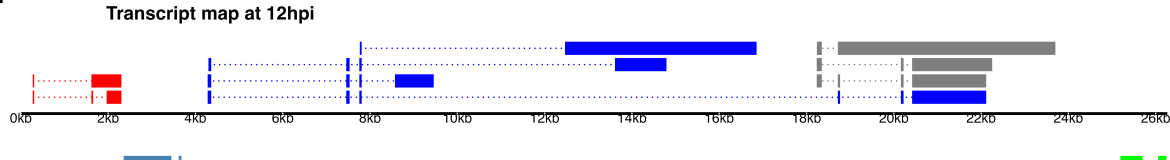
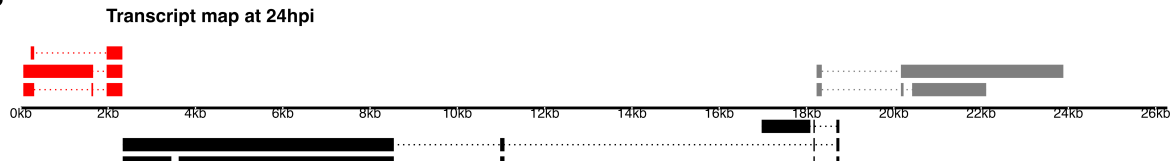
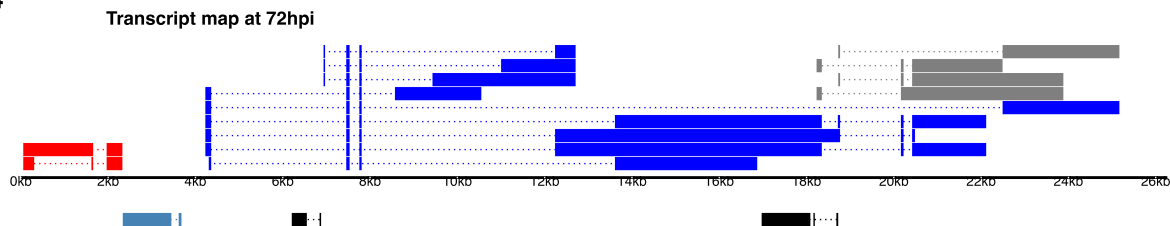
A**1****2****3****4**

Figure 3. A) Transcriptome of THEV from RNA-seq. THEV transcripts assembled from all time points by StringTie are unified forming this transcriptome (splicing map). Transcripts belonging to the same transcription unit (TU) are located in close proximity on the genome and are color coded and labeled in this figure as such. The organization of TUs in the THEV genome is unsurprisingly similar to MAdVs; however, the MAdV genome shows significantly more transcripts. The TUs are color coded: E1 transcripts - red, E2 - black, E3 - dark grey, E4 - green, MLTU - blue. Predicted ORFs are also indicated here, colored light grey. **B) THEV transcripts identified at given time points.** Transcripts are color coded as explained in (A).

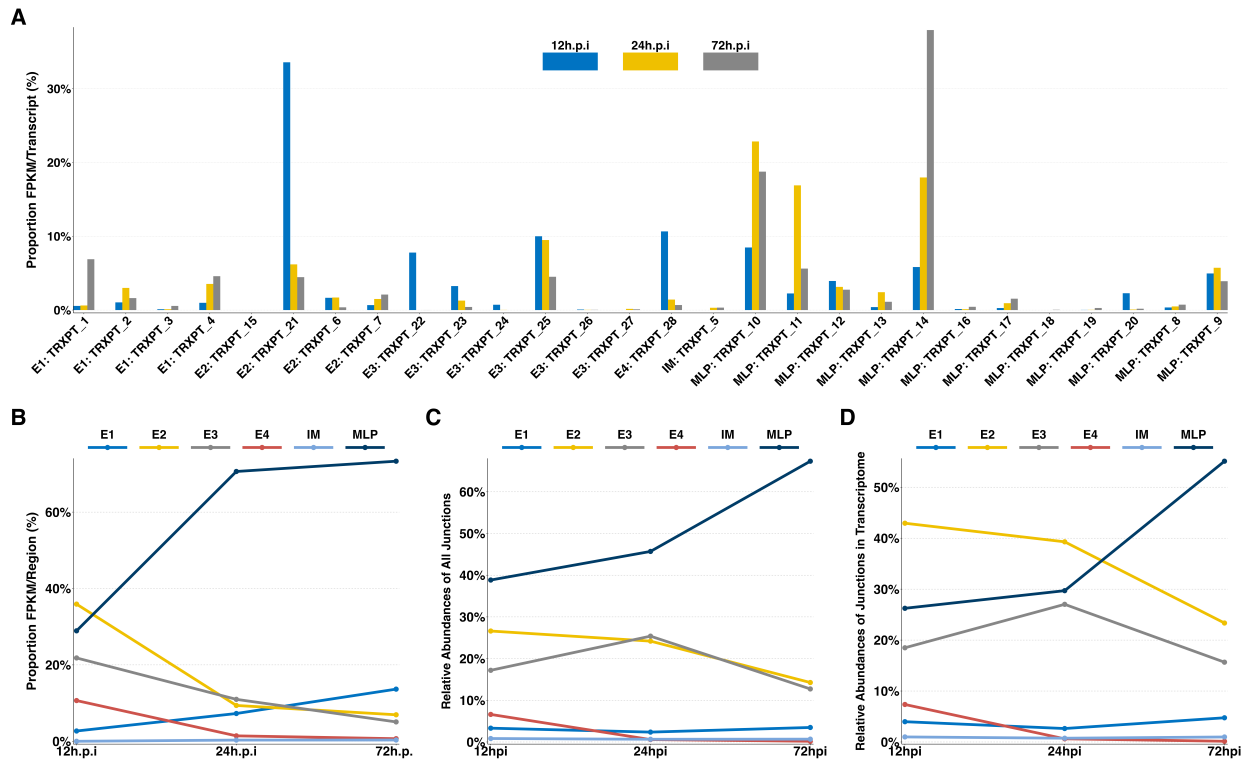


Figure 4: Changes in splicing and expression profile of THEV over time. **A) Normalized (FPKM) expression levels of transcripts over time.** The expression levels (FPKM) of individual transcripts as a percentage of the total expression of all transcripts at each time point are indicated. Only transcripts from our RNA-seq data are included here. **B) Normalized (FPKM) expression levels of transcripts by region over time.** The expression levels of each region/TU as a percentage of the total expression of all transcripts at each time point are indicated. Region expression levels were calculated by summing up the FPKMs of all transcripts categorized in that region. **C) Relative abundances of all splice junctions grouped by region/TU over time.** After assigning all 2,457 unique junctions to a TU and the total junction reads counted at each time point for each region, the total junction reads for each TU were plotted as percentages of all junction reads at each time point. Note that the junction read counts are not normalized. **D) Relative abundances of junctions in transcriptome grouped by region/TU over time.** This is identical to (C), except that only the junctions found in the full transcriptome obtained from the RNA-seq data were included.

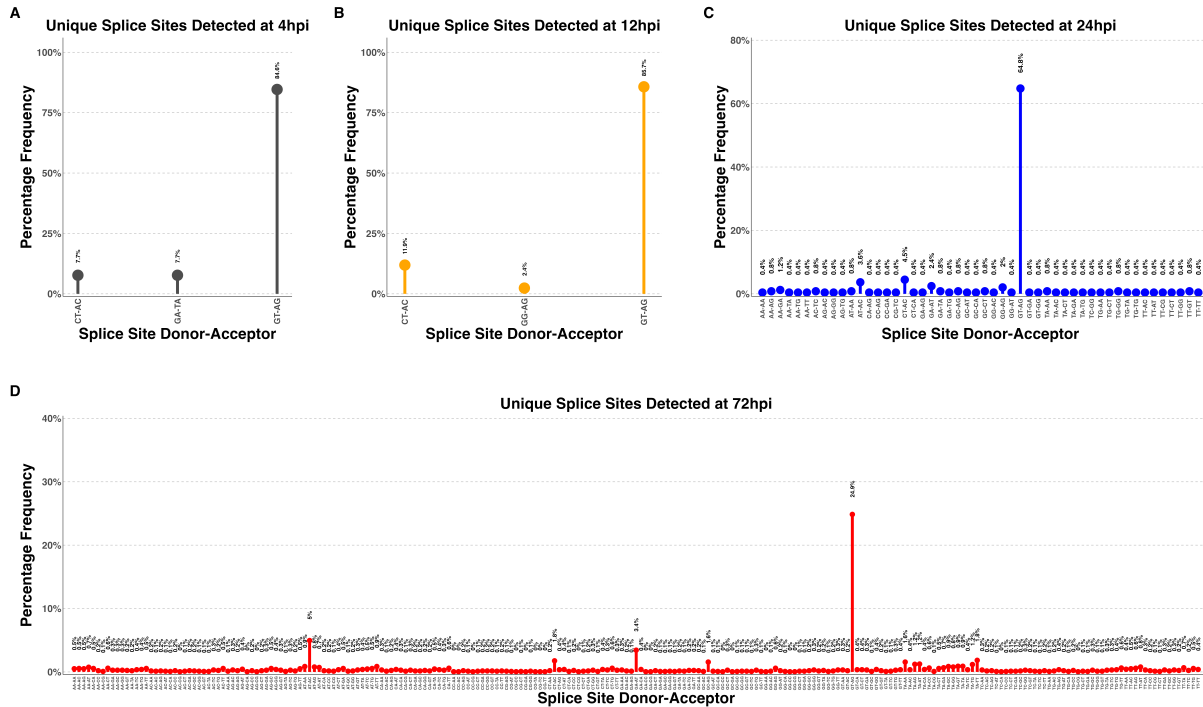
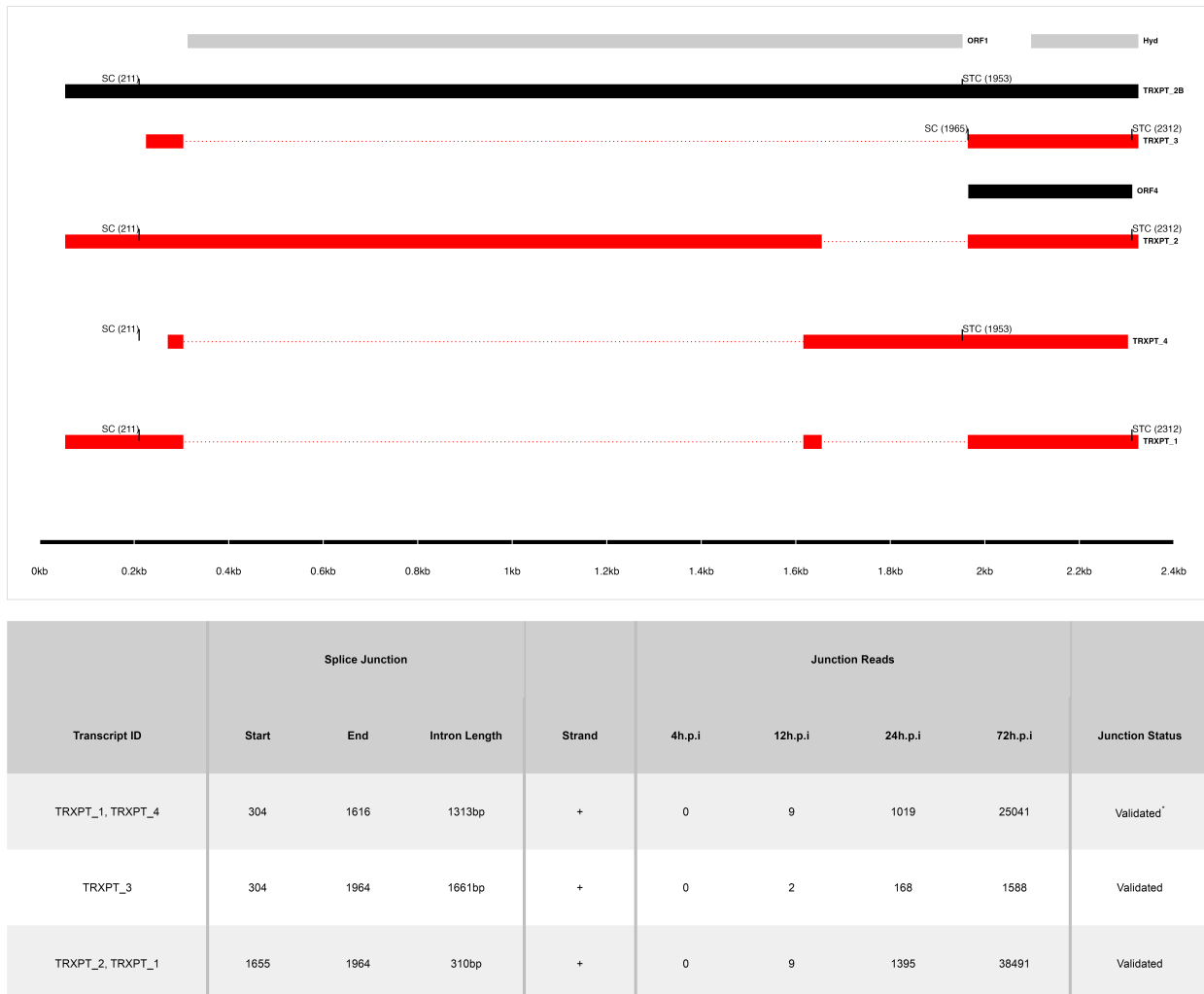
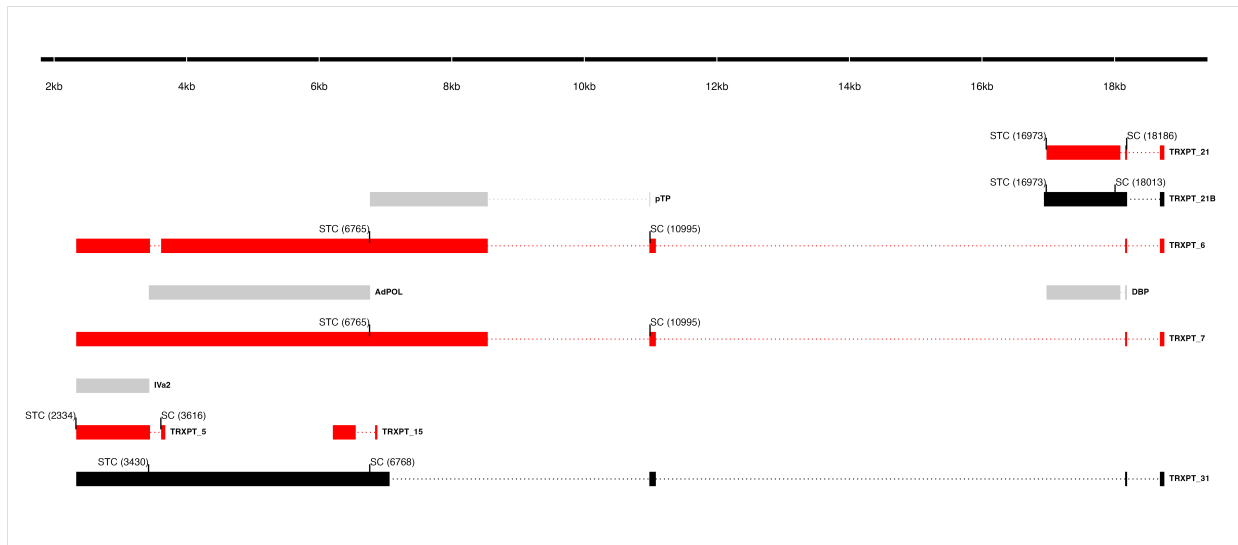


Figure 5: Changes in splice donor-acceptor nucleotides over time. The splice donor-acceptor nucleotides of THEV just like other AdVs is mostly the canonical GU-AG. At early time points (4h.p.i and 12h.p.i **(A)** and **(B)**, respectively) the junction nucleotides used appear to be well scrutinized or restricted, utilizing mostly the canonical splice nucleotides. However, as the infection progresses to the late stages (24h.p.i and 72h.p.i **(C)** and **(D)**, respectively), the selectivity of specific splice acceptor-donor pairs seems to degenerate significantly, such that all combinations of nucleotides are utilized.



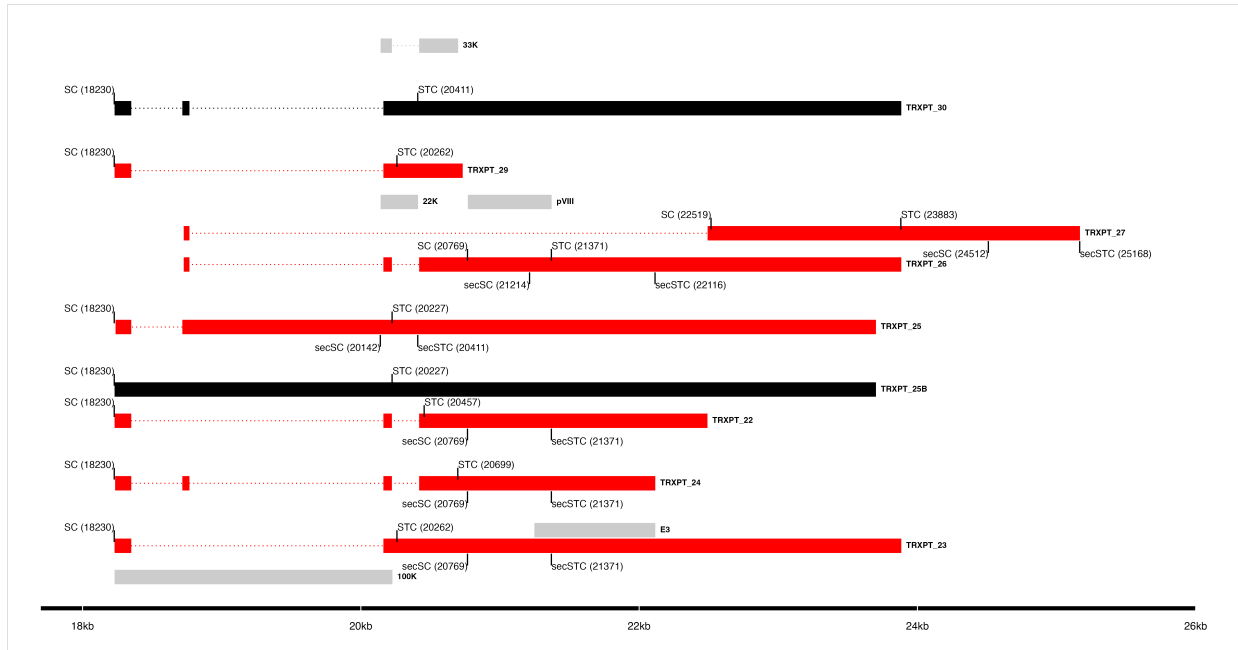
^{*}Not validated for TRXPT_4

Figure 6: The splice map of the E1 transcription unit (TU). Exons are depicted as boxes connected by introns (dotted lines). Transcripts from RNA-seq data are colored red, predicted ORFs are colored grey, and transcripts or ORFs discovered by other means are colored black. Each transcript or ORF is labelled with its name to the right. The start codon (SC) and stop codon (STC) of the 5'-most CDS of each transcript is indicated with the nucleotide position in brackets. The region of the virus is depicted at the bottom as a black line with labels of the nucleotide positions for reference. The table shows sequence reads covering the splice junctions with information about their validation status using cloning and Sanger sequencing.



Transcript ID	Splice Junction				Junction Reads					Junction Status
	Start	End	Intron Length	Strand	4h.p.i	12h.p.i	24h.p.i	72h.p.i		
TRXPT_5, TRXPT_7	3447	3615	169bp	-	1	5	720	13422	Validated	
TRXPT_6, TRXPT_7	11079	18159	7081bp	-	0	2	0	0	Validated	
TRXPT_21	18087	18159	73bp	-	9	103	0	0	Validated	
TRXPT_21, TRXPT_6, TRXPT_7	18189	18684	496bp	-	0	111	18794	156037	Validated	
TRXPT_6, TRXPT_7	8543	10981	2439bp	-	0	0	298	850	Validated	
TRXPT_15	6551	6843	293bp	-	0	0	0	6	Validated	

Figure 7: The splice map of the E2 and IM TUs. Exons are depicted as boxes connected by introns (dotted lines). Red transcripts are generated from RNA-seq data and predicted ORFs are colored grey. TRXPT_21B discovered by 3'RACE is colored black. Each transcript or ORF is labelled with its name to the right. The SC and STC of the 5'-most CDS of each transcript are indicated with the nucleotide position in brackets. The region of the virus is depicted at the bottom as a black line with labels of the nucleotide positions for reference. The table shows sequence reads covering the splice junctions with information about their validation status using cloning and Sanger sequencing.



Transcript ID	Splice Junction				Junction Reads					Junction Status
	Start	End	Intron Length	Strand	4h.p.i	12h.p.i	24h.p.i	72h.p.i		
TRXPT_25, TRXPT_24, TRXPT_10	18350	18717	368bp	+	4	21	3930	35490	Validated	
TRXPT_23, TRXPT_22, TRXPT_11	18350	20162	1813bp	+	3	18	6619	38841	Validated	
TRXPT_26, TRXPT_24, TRXPT_13, TRXPT_9, TRXPT_10	18768	20162	1395bp	+	2	21	5207	45062	Validated	
TRXPT_26, TRXPT_22, TRXPT_24, TRXPT_13, TRXPT_9, TRXPT_10	20223	20419	197bp	+	3	33	10583	93238	Validated	
TRXPT_27	18768	22492	3725bp	+	0	0	101	1950	Validated	

Figure 8: The splice map of the E3 TU. Exons are depicted as boxes connected by introns (dotted lines). Red transcripts are generated from RNA-seq data and predicted ORFs are colored grey. Transcripts discovered by other means are colored black. Each transcript or ORF is labelled with its name to the right. The start codon (SC) and stop codon (STC) of the 5'-most CDS of each transcript are indicated with the nucleotide position in brackets. Similarly, the secondary SC (secSC) and secondary STC (secSTC) are shown. The region of the virus is depicted at the bottom as a black line with labels of the nucleotide positions for reference. The table shows sequence reads covering the splice junctions with information about their validation status using cloning and Sanger sequencing.

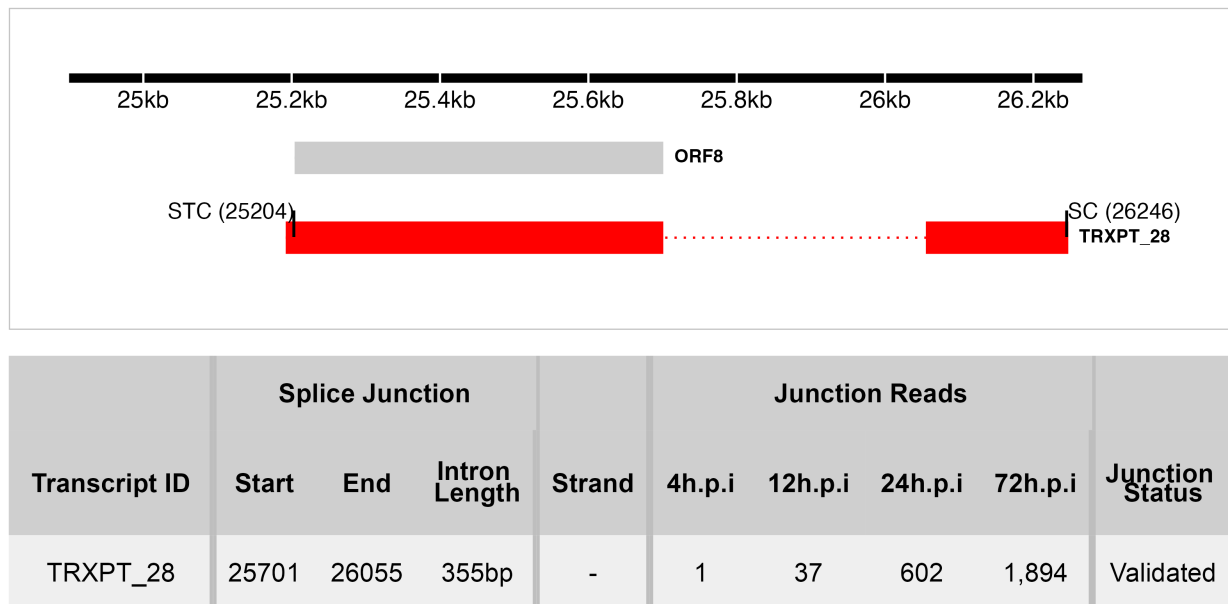
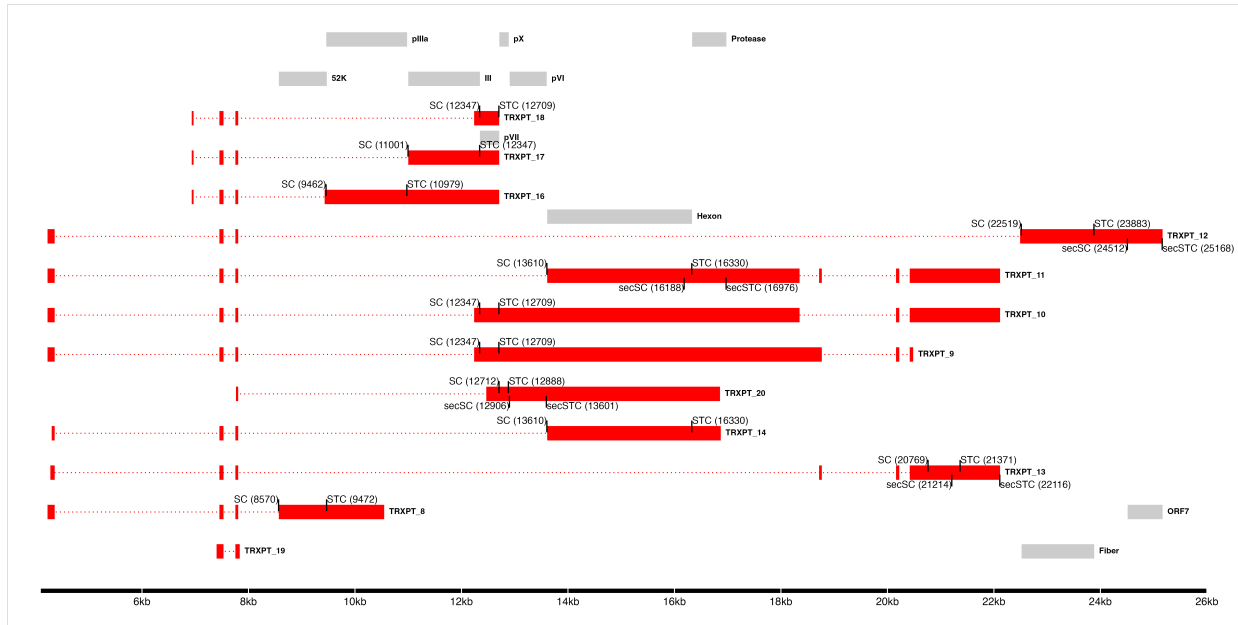


Figure 9: The splice map of the E4 TU. Exons are depicted as boxes connected by introns (dotted lines). The transcript from RNA-seq data is colored red and the predicted ORF, grey. The transcript and ORF are labelled with their names to the right. The start codon (SC) and stop codon (STC) of the 5'-most CDS are indicated with the nucleotide position in brackets. The region of the virus is depicted at the bottom as a black line with labels of the nucleotide positions for reference. The table shows sequence reads covering the splice junction with its validation status using cloning and Sanger sequencing.



Transcript ID	Splice Junction				Strand	Junction Reads				Junction Status
	Start	End	Intron Length			4h.p.i	12h.p.i	24h.p.i	72h.p.i	
TRXPT_13, TRXPT_8, TRXPT_14, TRXPT_10, TRXPT_12, TRXPT_11, TRXPT_9	4360	7454	3095bp		+	1	32	7128	179607	Validated
TRXPT_19, TRXPT_13, TRXPT_8, TRXPT_14, TRXPT_10, TRXPT_16, TRXPT_12, TRXPT_17, TRXPT_18, TRXPT_11, TRXPT_9	7531	7754	224bp		+	4	58	12319	322677	Validated
TRXPT_8	7807	8570	764bp		+	0	5	707	0	Validated
TRXPT_16	7807	11001	3195bp		+	0	1	226	10254	Validated
TRXPT_18, TRXPT_11, TRXPT_9	7807	12238	4432bp		+	0	7	2446	0	Validated
TRXPT_20	7807	12466	4660bp		+	0	3	437	0	Validated
TRXPT_14, TRXPT_10	7807	13610	5804bp		+	0	18	2553	0	Validated
TRXPT_13	7807	18717	10911bp		+	0	2	1391	0	Validated
TRXPT_12	7807	22492	14686bp		+	1	6	1642	21891	Validated
TRXPT_25, TRXPT_24, TRXPT_10	18350	18717	368bp		+	4	21	3930	35490	Validated
TRXPT_23, TRXPT_22, TRXPT_11	18350	20162	1813bp		+	3	18	6619	38841	Validated
TRXPT_26, TRXPT_24, TRXPT_13, TRXPT_9, TRXPT_10	18768	20162	1395bp		+	2	21	5207	45062	Validated
TRXPT_26, TRXPT_22, TRXPT_24, TRXPT_13, TRXPT_11, TRXPT_9, TRXPT_10	20223	20419	197bp		+	3	33	10583	93238	Validated
TRXPT_16, TRXPT_17, TRXPT_18	6969	7454	486bp		+	0	0	143	13482	Validated
TRXPT_17	7807	9430	1624bp		+	0	0	67	0	Validated

Figure 10: The splice map of the MLTU. Exons are depicted as boxes connected by introns (dotted lines). The transcripts from our RNA-seq data are colored red and the predicted ORFs, grey. The transcripts and ORFs are labelled with their names to the right. The start codon (SC) and stop codon (STC) of the 5'-most CDS of each transcript is indicated with the nucleotide position in brackets. Similarly, the secondary SC (secSC) and secondary STC (secSTC) are shown. The region of the virus is depicted at the bottom as a black line with labels of the nucleotide positions for reference. The table shows sequence reads covering the splice junctions with information about their validation status using cloning and Sanger sequencing.

Table 1: Overview of sequencing results

Metric	4h.p.i	12h.p.i	24h.p.i	72h.p.i	Total
Total reads	1.17e+08	7.63e+07	1.20e+08	1.15e+08	4.28e+08
Mapped (Host)	1.04e+08	6.79e+07	1.06e+08	8.38e+07	3.62e+08
Mapped (THEV)	4.32e+02	6.70e+03	1.18e+06	1.69e+07	1.81e+07
Mean Per Base Coverage/Depth	2.42	37.71	6,666.96	95,041.7	101,749
Total unique splice junctions	13	37	236	2374	2,457
Junction coverage Total (at least 1 read)	37	605	115075	2132806	2.25e+06
Junction coverage Mean reads	2.8	16.4	487.6	898.4	351.3
Junction coverage (at least 10 reads)	0	13	132	1791	1,936
Junction coverage (at least 100 reads)	0	1	53	805	859
Junction coverage (at least 1000 reads)	0	0	18	168	186

Table 2a: Most abundant splice junctions at 12h.p.i

Timepoint	Strand	Start	End	Region	Intron Length	Reads (Percentage)
12hpi	-	18,087	18,159	E2	72 bp	103 (17%)
12hpi	+	18,189	18,684	MLP	495 bp	97 (16%)
12hpi	+	7,531	7,754	MLP	223 bp	58 (9.6%)
12hpi	-	25,701	26,055	E4	354 bp	37 (6.1%)
12hpi	+	20,223	20,419	E3	196 bp	33 (5.5%)
12hpi	+	4,360	7,454	MLP	3,094 bp	32 (5.3%)
12hpi	-	18,751	20,668	E2	1,917 bp	22 (3.6%)
12hpi	+	18,350	18,717	E3	367 bp	21 (3.5%)
12hpi	+	18,768	20,162	E3	1,394 bp	21 (3.5%)
12hpi	+	7,807	13,610	MLP	5,803 bp	18 (3%)
12hpi	+	18,350	20,162	E3	1,812 bp	18 (3%)
12hpi	-	18,189	18,684	E2	495 bp	14 (2.3%)
12hpi	-	18,751	21,682	E2	2,931 bp	10 (1.7%)
12hpi	+	304	1,616	E1	1,312 bp	9 (1.5%)
12hpi	+	1,655	1,964	E1	309 bp	9 (1.5%)
12hpi	-	18,087	18,163	E2	76 bp	8 (1.3%)
12hpi	+	7,807	12,238	MLP	4,431 bp	7 (1.2%)
12hpi	+	7,807	22,492	MLP	14,685 bp	6 (1%)

Table 2b: Most abundant splice junctions at 24h.p.i

Timepoint	Strand	Start	End	Region	Intron Length	Reads (Percentage)
24hpi	-	18,087	18,159	E2	72 bp	18,825 (16.4%)
24hpi	+	18,189	18,684	MLP	495 bp	17,670 (15.4%)
24hpi	+	7,531	7,754	MLP	223 bp	12,319 (10.7%)
24hpi	+	20,223	20,419	E3	196 bp	10,583 (9.2%)
24hpi	+	4,360	7,454	MLP	3,094 bp	7,128 (6.2%)
24hpi	+	18,350	20,162	E3	1,812 bp	6,619 (5.8%)
24hpi	+	18,768	20,162	E3	1,394 bp	5,207 (4.5%)
24hpi	+	18,350	18,717	E3	367 bp	3,930 (3.4%)
24hpi	-	18,751	20,668	E2	1,917 bp	3,870 (3.4%)
24hpi	+	7,807	13,610	MLP	5,803 bp	2,553 (2.2%)
24hpi	+	7,807	12,238	MLP	4,431 bp	2,446 (2.1%)
24hpi	+	7,807	22,492	MLP	14,685 bp	1,642 (1.4%)
24hpi	+	1,655	1,964	E1	309 bp	1,395 (1.2%)
24hpi	+	7,807	18,717	MLP	10,910 bp	1,391 (1.2%)
24hpi	-	18,189	18,684	E2	495 bp	1,124 (1%)
24hpi	-	18,751	21,128	E2	2,377 bp	1,124 (1%)
24hpi	+	20,223	20,894	E3	671 bp	1,208 (1%)

Table 2c: Most abundant splice junctions at 72h.p.i

Timepoint	Strand	Start	End	Region	Intron Length	Reads (Percentage)
72hpi	+	7,531	7,754	MLP	223 bp	322,677 (15.1%)
72hpi	+	4,360	7,454	MLP	3,094 bp	179,607 (8.4%)
72hpi	-	18,087	18,159	E2	72 bp	161,336 (7.6%)
72hpi	+	18,189	18,684	MLP	495 bp	146,425 (6.9%)
72hpi	+	20,223	20,419	E3	196 bp	93,238 (4.4%)
72hpi	+	7,807	13,610	MLP	5,803 bp	81,420 (3.8%)
72hpi	+	7,807	12,238	MLP	4,431 bp	77,616 (3.6%)
72hpi	+	18,768	20,162	E3	1,394 bp	45,062 (2.1%)
72hpi	+	1,655	1,964	E1	309 bp	38,491 (1.8%)
72hpi	+	18,350	20,162	E3	1,812 bp	38,841 (1.8%)
72hpi	+	18,350	18,717	E3	367 bp	35,490 (1.7%)
72hpi	+	304	1,616	E1	1,312 bp	25,041 (1.2%)
72hpi	-	18,751	20,668	E2	1,917 bp	26,338 (1.2%)
72hpi	+	7,807	12,904	MLP	5,097 bp	21,946 (1%)
72hpi	+	7,807	22,492	MLP	14,685 bp	21,891 (1%)

530 **SUPPLEMENTARY MATERIALS**

531 **Supplementary Table S1A**

Table S1a: Most Transcriptionally Active Regions of THEV at 12h.p.i

Time	Region	Strand	Total Reads	Percentage
12hpi	MLP	+	235	38.8%
12hpi	E2	-	161	26.6%
12hpi	E3	+	104	17.2%
12hpi	E4	-	40	6.6%
12hpi	Unassigned	-,+/-	40	6.6%
12hpi	E1	+	20	3.3%
12hpi	IM	-	5	0.8%

532 **Supplementary Table S1B**

Table S1b: Most Transcriptionally Active Regions of THEV at 24h.p.i

Time	Region	Strand	Total Reads	Percentage
24hpi	MLP	+	52,589	45.7%
24hpi	E3	+	29,208	25.4%
24hpi	E2	-	27,833	24.2%
24hpi	E1	+	2,724	2.4%
24hpi	Unassigned	-,+/-	1,313	1.1%
24hpi	IM	-	744	0.6%
24hpi	E4	-	664	0.6%

⁵³³ **Supplementary Table S1C**

Table S1c: Most Transcriptionally Active Regions of THEV at 72h.p.i

Time	Region	Strand	Total Reads	Percentage
72hpi	MLP	+	1,436,199	67.3%
72hpi	E2	-	304,191	14.3%
72hpi	E3	+	271,310	12.7%
72hpi	E1	+	74,135	3.5%
72hpi	Unassigned	-,+/-	28,921	1.4%
72hpi	IM	-	14,482	0.7%
72hpi	E4	-	3,568	0.2%

⁵³⁴ **Supplementary Table S2**

Table S2: Mapping Transcript TTS with Closest Polyadenylation Signal

Region	Sub Region	Transcripts	Nearest 'AAUAAA' TTS	
			TTS	signal (location refers to 'U' in the sequence)
E1	E1	TRXPT_1, TRXPT_2, TRXPT_3, TRXPT_4	2,325	2,323
E2	E2A	TRXPT_21, TRXPT_21B	16,934	16,950
E2/IM	E2B/IM	TRXPT_5, TRXPT_6, TRXPT_7, TRXPT_31	2,334	2,333
E3	E3A	TRXPT_22, TRXPT_24	22,491	22,458 (AGUAAA)

Table S2: Mapping Transcript TTS with Closest Polyadenylation Signal

Region	Sub Region	Transcripts	TTS	Nearest 'AAUAAA' TTS signal (location refers to 'U' in the sequence)
E3	E3B	TRXPT_23, TRXPT_25, TRXPT_25B, TRXPT_26, TRXPT_30	23,884	23,889
E3	E3C	TRXPT_27	25,168	25,166
E4	E4	TRXPT_28	25,192	25,203
MLTU	L1	TRXPT_8	10,549	10,537
MLTU	L2	TRXPT_16, TRXPT_17	12,709	-
MLTU	L3	TRXPT_14, TRXPT_20	16,870	16,903
MLTU	L4	TRXPT_9, TRXPT_10, TRXPT_11, TRXPT_13	22,116	22,098 (AAGAAA)
MLTU	L5	TRXPT_12	25,168	25,166

535 **Supplementary Table S3**

Table S3: The Encoded Proteins and Coding Potential of THEV Transcripts

mRNA	Primary Product	Size (kDa)	Number of Residues	Start Codon Position	Stop Codon Position	Downstream Coding Potential
TRXPT_1	ORF9 ^{new}	17.9	160	211	2312	Hyd, ORF4
TRXPT_2	ORF10 ^{new}	66.4	597	211	2312	Hyd, ORF4
TRXPT_2B	eORF1 ^L	64.3	580	1965	1953	Hyd, ORF4
TRXPT_3	ORF4	13.1	115	211	2312	Hyd

Table S3: The Encoded Proteins and Coding Potential of THEV Transcripts

mRNA	Primary Product	Size (kDa)	Number of Residues	Start Codon Position	Stop Codon Position	Downstream Coding Potential
TRXPT_4	ORF11 ^{new}	15.9	143	211	1953	Hyd, ORF4
TRXPT_5	IVa2	42.3	371	3616	2334	-
TRXPT_6	pTP	70.5	597	10995	6765	Ad-pol
TRXPT_7	pTP	70.5	597	10995	6765	Ad-pol
TRXPT_8	52K	33.8	300	8570	9472	-
TRXPT_9	pVII	13.2	120	12347	12709	pX, pVI, hexon, eProt, ORF12, pVIII, eE3
TRXPT_10	pVII	13.2	120	12347	12709	pX, pVI, hexon, eProt, ORF12, pVIII, eE3
TRXPT_11	Hexon (II)	101.1	906	13610	16330	eProt, ORF12, e33K, pVIII, eE3
TRXPT_12	Fiber (IV)	49	454	22519	23883	ORF7
TRXPT_13	pVIII	21.8	200	20769	21371	eE3
TRXPT_14	Hexon (II)	101.1	906	13610	16330	-
TRXPT_15	-	-	-	-	-	-
TRXPT_16	pIIIa	57.6	505	9462	10979	Penton (III), pVII
TRXPT_17	Penton (III)	50.8	448	11001	12347	-
TRXPT_18	pVII	13.2	120	12347	12709	-
TRXPT_19	-	-	-	-	-	-
TRXPT_20	pX	6.1	58	12712	12888	pVI, hexon

Table S3: The Encoded Proteins and Coding Potential of THEV Transcripts

mRNA	Primary Product	Size (kDa)	Number of Residues	Start Codon Position	Stop Codon Position	Downstream Coding Potential
TRXPT_21	DBP	43.3	380	18186	16973	-
TRXPT_21B	tDBP ^S	39.3	346	18013	16973	-
TRXPT_22	8.3KII ^{new}	8.6	73	18230	20457	pVIII, eE3
TRXPT_23	8.3KI ^{new}	8.3	73	18230	20262	pVIII, eE3, Fiber
TRXPT_24	e33K ^L	19.8	171	18230	20699	pVIII, E3
TRXPT_25	t100K	62.4	543	18230	20227	22K, pVIII, eE3
TRXPT_25B	100K	76.5	665	18230	20227	22K, pVIII, eE3
TRXPT_26	pVIII	21.8	200	20769	21371	eE3, Fiber
TRXPT_27	Fiber (IV)	49	454	22519	23883	ORF7
TRXPT_28	eORF8 ^L	26.4	229	26246	25204	-
TRXPT_29	8.3KI	8.3	73	18230	20262	-
TRXPT_30	e22K ^L	15.7	140	18230	20411	pVIII, eE3, Fiber
TRXPT_31	Ad-pol	129.2	1112	6768	3430	-

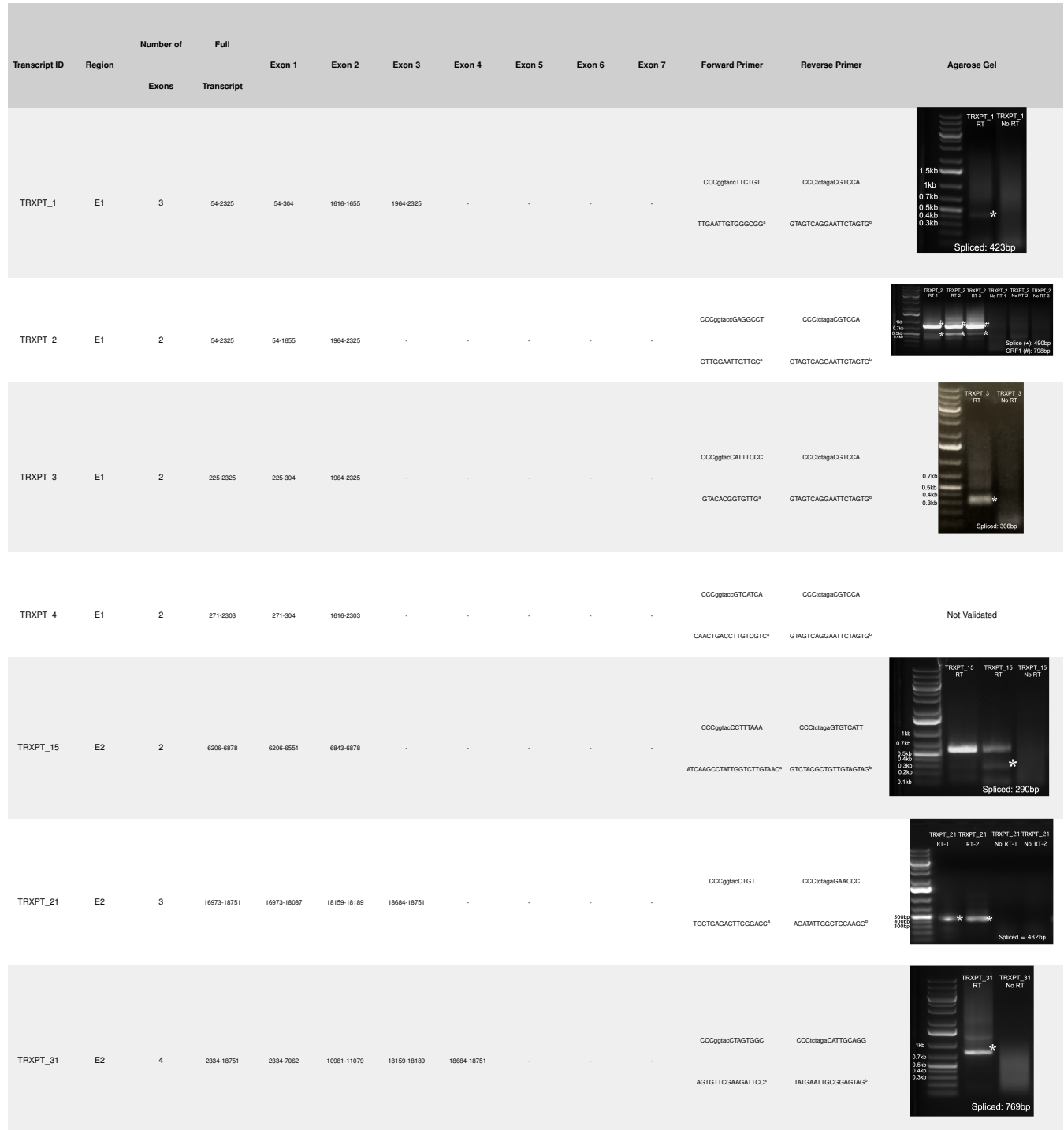
^{new}Novel product identified in this work;

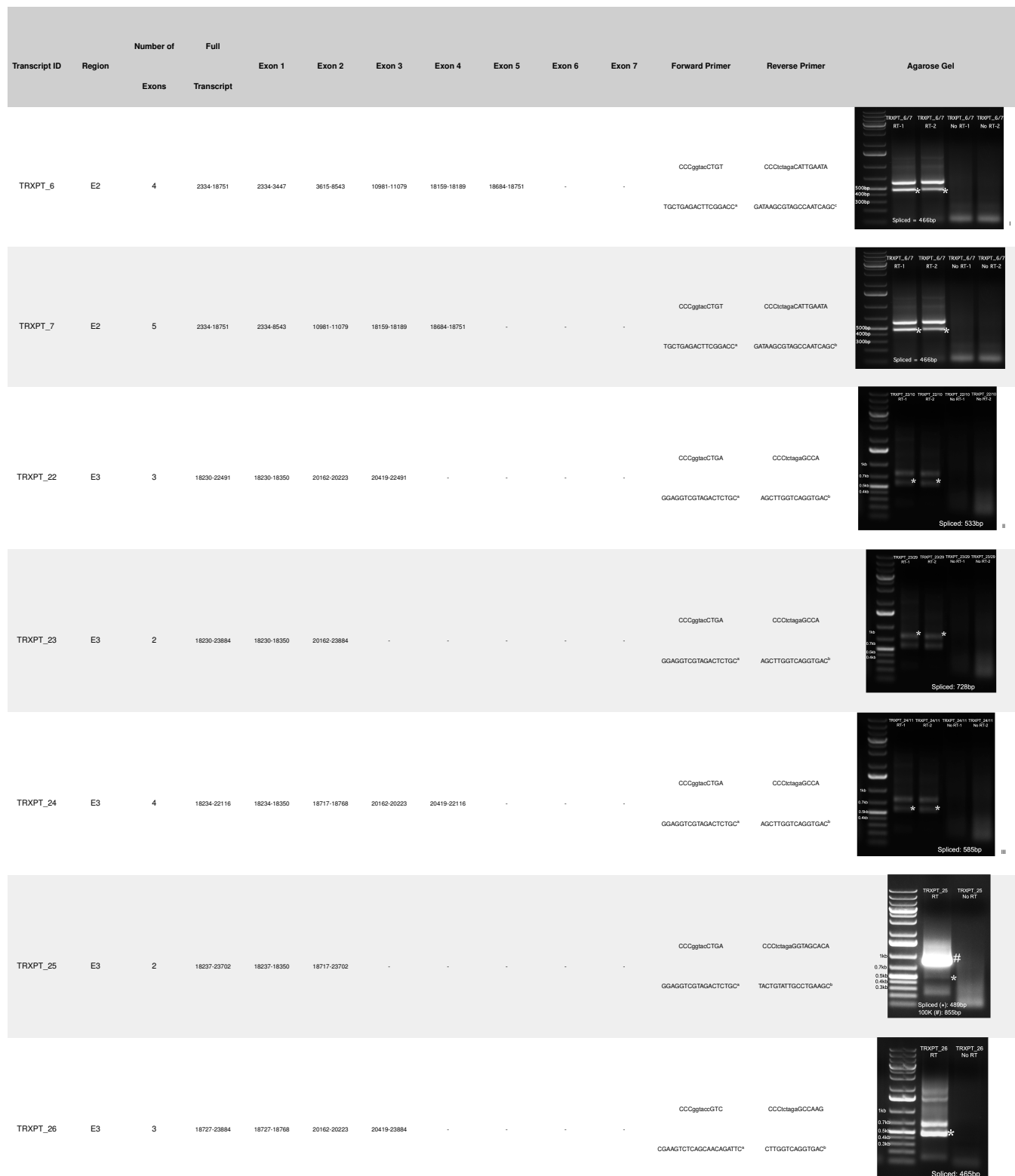
^LLonger isoform identified in this work

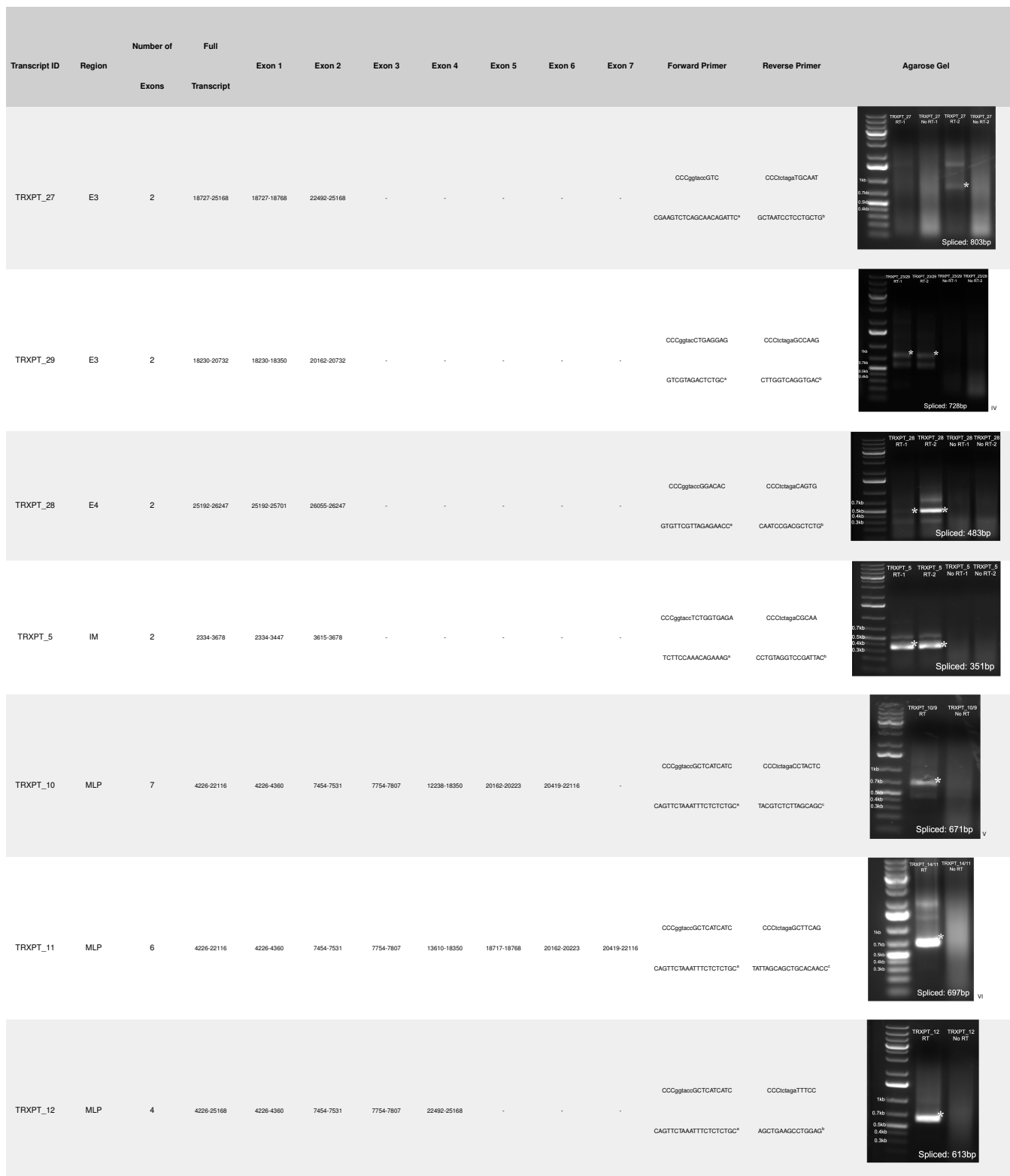
^SShorter isoform identified in this work

536 **Supplementary PCR Methods**

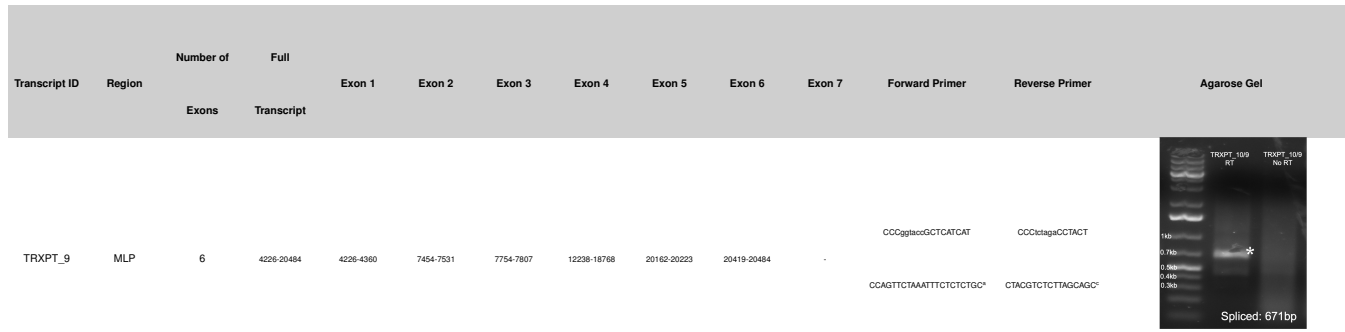
Agarose Gels Showing PCR Amplification of THEV cDNA With Gene-Specific Primers







Transcript ID	Region	Number of Exons	Full Transcript							Forward Primer	Reverse Primer	Agarose Gel
			Exon 1	Exon 2	Exon 3	Exon 4	Exon 5	Exon 6	Exon 7			
TRXPT_13	MLP	6	4279-22116	4279-4360	7454-7531	7754-7807	18717-18768	20162-20223	20419-22116	CCGgttaccGCTCATCATC	CCCttagaGCCAAG	
TRXPT_14	MLP	4	4304-16870	4304-4360	7454-7531	7754-7807	13610-16870	-	-	CCGgttaccGCTCATCATC	CCCttagaGCTTCAGT	
TRXPT_16	MLP	4	6934-12709	6934-6969	7454-7531	7754-7807	9430-12709	-	-	CCGgttaccGGATCTC	CCCttagaGCCT	
TRXPT_17	MLP	4	6934-12709	6934-6969	7454-7531	7754-7807	11001-12709	-	-	CCGgttaccGGATCTC	CTCCCCATCTAGAC	
TRXPT_18	MLP	4	6934-12709	6934-6969	7454-7531	7754-7807	12238-12709	-	-	CCGgttaccGGATCTC	CCCttagaGTTCTC	
TRXPT_19	MLP	2	7401-7836	7401-7531	7754-7836	-	-	-	-	-	-	N/A
TRXPT_20	MLP	2	7765-16856	7765-7807	12466-16856	-	-	-	-	CCGgttaccGAGGATTGA	CCCttagaCTGAA	
TRXPT_8	MLP	4	4226-10549	4226-4360	7454-7531	7754-7807	8570-10549	-	-	CCGgttaccGCTCATCAT	CCCttagaCCTATC	



^aPrimer binds inside first exon; ^bPrimer binds inside terminal exon; ^cPrimer binds inside fourth exon; ^dAgarose gel identical to TRXPT_7 due to identical splicing; ^eAgarose gel identical to last 3 exons of TRXPT_10 due to identical splicing; ^fAgarose gel identical to last 4 exons of TRXPT_11 due to identical splicing; ^gAgarose gel identical to TRXPT_23 due to identical splicing; ^hAgarose gel identical to TRXPT_9 due to identical splicing; ⁱAgarose gel identical to TRXPT_14 due to identical splicing;

537 In the table above, the restriction sites in the primer tails are shown in lowercase letters. All the primer melting
 538 temperatures (TMs) are 58-60°C using a hot start Taq DNA polymerase. The PCR reaction mix was made
 539 per manufacturer's instructions. The PCR cycling conditions were as follows: Initial denaturation – 95°C for
 540 1 minute; cyclical denaturation – 95°C for 30 seconds, annealing – variable temperature (53°C-56°C) for
 541 30 seconds, primer extension – 68°C for variable time, and final elongation – 68°C for 5 minutes. We used
 542 35 cycles of amplification. The PCR products of THEV cDNA shown in the gels in the table above were
 543 cloned and Sanger sequenced to confirm the splice junctions. We included "No reverse transcriptase (No
 544 RT)" template controls to ensure the PCR products are of RNA origin.

545 **Supplementary Computational Analysis**

546 Snakemake v7.24.0 was used to manage our entire workflow. A graph of the main steps in our pipeline
 547 generated with Snakemake is shown below. Our trimmed RNA-seq reads were mapped to the genome of
 548 *M. gallopano* (with the THEV genome as one of its chromosomes) using Hisat2, to generate the alignment
 549 (BAM) files and StringTie used to assemble the transcriptome with a GTF annotation file containing the
 550 predicted THEV ORFs as a guide. The GTF annotation file was derived from a GFF3 annotation file obtained
 551 from NCBI using Agat - version 1.0.0, a program for converting between many different file formats used in
 552 bioinformatics. However, the NCBI GFF3 annotation file itself was first modified to remove all unimportant
 553 features, leaving only the ORFs.

554 StringTie was also used to estimate the normalized expression levels (FPKM) of all the transcripts and
 555 Ballgown in R was used to perform statistical analysis and comparisons of the transcript expression levels,
 556 which was instructive in understanding the temporal regulation THEV gene expression.

557 In these steps above, each sample (replicate of each time point) was processed independently and merged
 558 only in the final transcriptome assembly or during analysis with Ballgown. In the subsequent steps described

559 below, all samples for each time point were processed together.

560 We used RegTools to extract and analyze the splice junctions in the BAM files. The command “regtools
561 junctions extract” provides a wealth of information about all the splice sites in the BAM file provided such as:
562 the start and end positions, the strand, and number of reads supporting the splice junctions. The command
563 “regtools junctions annotate” gives even more information such as: the splice site donor-acceptor sequences
564 and transcripts/genes that overlap the junction. This information was the basis for estimating and comparing
565 the splicing activity of different regions (TUs) of THEV over time. Also, Samtools was also used to count the
566 total sequencing reads for all replicates at each time point.



A flowchart of the major steps in the computational analysis pipeline (*generated with Snakemake*)